Department of Chemical Engineering

The Inhibition Performance of Poly(ethylene oxide-co-vinylpyrrolidone) in the Presence of Thermodynamic Hydrate Inhibitors

Xinyu Li

This thesis is presented for the Degree of

Master of Philosophy

of

Curtin University

June 2018

Declaration

To the best of my knowledge and belief this thesis contains no materials previously published by any other person except where due acknowledgement has been made.

This thesis contains no material which has been accepted for the award of any other degree or diploma in any university.

Signature: 

Date: 26th June 2018

Acknowledgements

Over the period of my research work, I have been privileged to receive the support of my supervisors, friends and family.

Firstly, I would like to express my sincere gratitude to my supervisor, Professor Xia Lou, for her continuous help, invaluable advice, motivation and guidance. I am extremely lucky to be her student. She has tried the hardest to pass on her research experience and knowledge to me. It would never have been possible for me to complete this work without her wealth of knowledge and unbelievable work ethic. I also benefited from discussions with my co-supervisor, Associate Professor Zachary Aman.

My sincere appreciation also goes to my friend, Dr. Chao Su, for her support not only in providing technical advice but also in sharing her own experiences to fight the challenges offered by research. She inspired me in many ways to face all the difficulties fearlessly.

Finally, I would like to thank my parents, Min and Guizhi, as well as my husband, Chong, for their unconditional support, love and encouragement. With them always behind me, I was able to concentrate on my studies without distraction. This work is also for my little boy, Liam, and my daughter-to-be, Lexi. They provide the true strength that powers me up to chase my dreams.

Abstract

Natural gas hydrates pose a significant hazard to drilling and production operations within the oil and gas industry. Injections of thermodynamic hydrate inhibitors (TIs) such as mono-ethylene glycol (MEG) and methanol (MeOH) are widely used by the industry to mitigate formation of gas hydrates. This method is proven to be effective. However, the high cost associated with the large quantities of TIs being used, and growing concerns about the negative impact of the chemical reagents upon the environment have led to continuous efforts to seek out and develop alternatives. Kinetic hydrate inhibitors (KHIs) have been found to be able to delay gas hydrates formation at a concentration below 1% but show limited effectiveness for high subcooling. Investigations into the synergistic effect of TIs in combination with KHIs have attracted increasing attention over recent years.

The aim of this thesis is to investigate the possible synergistic effect on the inhibition of natural gas hydrates by MEG and methanol in the presence of poly(ethylene oxide-co-vinylpyrrolidone) (PEO-co-VP), a KHI designed and synthesised by the same research group.

A sapphire high pressure cell was used to carry out the hydrates formation experiments involving synthetic natural gas made of methane, ethane and propane in a molar ratio of 92:5:3, and a 3.5% sodium chloride solution. The onset time, growth time, gas consumption and percentage of hydrate conversion were used to evaluate the overall inhibition performance of the pure KHI, as well as the combined KHI and TI systems. The effects of the KHI, the TIs, and the combined KHI and TI of varying concentrations, and the degree of subcooling on the aforementioned parameters, were investigated. The change of KHI concentration during the hydrates formation process was measured in order to understand the inhibition behaviour of the inhibitors.

The key findings of the project included:

- PEO-co-VP delayed the nucleation and reduced the growth of gas hydrates. The inhibition performance was not sensitive to the concentration change, up

to 1% at the selected subcooling temperature of 12.9°C. Little inhibition was observed when KHI concentration was increased to 1.5%, likely due to the catastrophic growth of natural gas hydrates. At the same sub–cooling level, both MEG and MeOH showed a concentration-dependent synergistic effect with PEO-co-VP on hydrate inhibition. Significant synergy was observed when 15% of MEG or 10% MeOH was added into 1% of the KHI. Higher TIs were required at a lower KHI concentration.

- In the absence of TI, a time-dependent ***decrease*** of KHI concentration in the liquid phase was observed during the hydrate-forming process. However, in the presence of the TI, KHI concentrations ***increased*** with time. The results indicate strong molecular interactions between the KHI and TIs.
- The effect of subcooling on the onset time followed a similar trend in the systems including the blank solution, the solution containing KHI alone, and the solution containing a mixture of KHI and TIs, which can be described by the Arrhenius equation.

Overall, the outcomes of this project have demonstrated apparent synergistic effects of both MEG and methanol when combined with the KHI that contains PEO and polyvinylpyrrolidone moieties, as a result of strong molecular interactions between the TIs and the KHI. The investigation also demonstrated that the synergistic effect was both concentration- and temperature-dependent. The findings are of significant value to both the gas hydrates science and engineering field of study, and the oil and gas industry.

Table of Contents

Declaration ..... **I**

Acknowledgements ..... **II**

Chapter 1 Introduction **2**

1.1 Natural Gas Hydrates 2

1.2 Chemical Inhibition of Natural Gas Hydrates 4

1.2.1 Thermodynamic inhibitors (TIs) 4

1.2.2 Low dosage hydrate inhibitors (LHDIs) 6

1.3 Synergists to the Inhibition Performance of KHIs 8

1.4 Scope of Work 11

Chapter 2 Experimental Set-up and Procedures **13**

2.1 Introduction 13

2.2 Chemicals and Materials 13

2.3 Experimental Set-up 14

2.3.1 High pressure cell 14

2.3.2 Temperature control bath 15

2.4 Experimental Procedures 17

2.5 Sample Extraction 19

2.6 Gas Consumption Calculation 20

2.7 Experimental Conditions 21

2.7.1 Agitation speed 21

2.7.2 Onset temperature 24

2.8 UV-Vis Spectroscopy 25

Chapter 3 Synergistic Effect of MEG with PEO-co-VP **28**

3.1 Inhibition Performance of PEO-co-VP in Absence of MEG 29

3.2 The Effect of MEG on the Inhibition Performance of KHI 32
3.2.1 Onset time 32
3.2.2 Hydrate growth time 36
3.2.3 The overall percentage of gas consumption 38
3.3 The Effect of KHI Concentration on the Overall Performance of Synergists 39
3.4 Temperature Effect on Inhibition Performance 41
3.4.1 PEO-co-VP without MEG 41
3.4.2 PEO-co-VP with 5% MEG 44
3.5 Conclusions 46
Chapter 4 Synergistic Effect of MeOH with PEO-co-VP 48
4.1 The Effect of MeOH on the Inhibition Performance of PEO-co-VP 48
4.1.1 Onset time 48
4.1.2 Hydrate growth and gas consumption 50
4.2 The Effect of KHI Concentration on the Overall Performance of Synergists 56
4.3 Conclusions 62
Chapter 5 Conclusions and Future Work 63
References 65
Appendix A: 74
Onset time (t_{onset}) and the corresponding subcooling temperature (T_{sc}) of various hydrate-forming solutions 74
Appendix B: 75
Onset time (t_{onset}) and the corresponding subcooling temperature (T_{sc}) of various hydrate-forming solutions at 2 ℃ 75
Appendix C: 78
Copyright agreement for Chapter 1 78

Copyright agreement for Chapter 4 80

List of Figures

Fig. 1.1 Basic cages of sI and sII hydrates (Obtained with permission from Lederhos et al., 1996)..... **3**

Fig. 1.2 Methane gas hydrate equilibrium curves with methanol concentrations of 0wt% (red), 0.05wt% (green), 0.10wt% (blue) and 0.20wt% (orange) in a 3.5wt% sodium chloride solution (predicted by GSMGem) (Obtained with permission from Lafond et al., 2012)..... **5**

Fig. 2.1 Chemical structure of PEO-co-VP..... **13**

Fig. 2.2 Schematic diagram of the high pressure cell with its accessories..... **15**

Fig. 2.3 Schematic diagram of temperature control bath..... **16**

Fig. 2.4 Complete assembly of experiment apparatus..... **16**

Fig. 2.5 Pressure-temperature-time (P-T-t) curves of the hydrate-forming solution containing 1% KHI..... **18**

Fig. 2.6 Determination of the onset temperature from the P-T-t curve of the hydrate-forming solution containing 1% KHI at 600 rpm..... **19**

Fig. 2.7 The time profiles of (a) pressure (P), (b) temperature (T), and (c) gas consumption in deionised water (30 ml) at various agitation speeds..... **22**

Fig. 2.8 Photographs showing hydrate formation at onset (a) and at 120 min after onset (b) at 200 rpm (30 mL DI water, T=2.0 °C, P=6.33 MPa)..... **23**

Fig. 2.9 UV-Vis spectrum for 0.01% PEO-co-VP solution..... **25**

Fig. 2.10 Calibration curve (PEO-co-VP in 3.5% NaCl)..... **26**

Fig. 2.11 Calibration curve (PEO-co-VP in 15% MEG)..... **27**

Fig. 2.12 Calibration curve (PEO-co-VP in 15% MeOH)..... **27**

Fig. 3.1 The effect of PEO-co-VP concentration on (a) onset time, (b) growth time and (c) percentage of gas consumption..... **30**

Fig. 3.2 The percentage of hydrate conversion with PEO-co-VP concentrations of 0.5%, 1% and 1.5%..... **32**

Fig. 3.3 Onset time for 0.5% PEO-co-VP and MEG of varying concentrations..... **33**

Fig. 3.4 The onset time for 1% PEO-co-VP and MEG of varying concentrations..... **34**

Fig. 3.5 PEO-co-VP concentrations during hydrate growth in (a) 0.5% KHI and (b) 0.5% + 15% MEG solutions **38**
Fig. 3.6 Percentage of gas consumption (N) of 0.5% KHI and 1% KHI with varying MEG concentrations **39**
Fig. 3.7 Onset time (t_{onset}) and growth time (Δt) of hydrate-forming solutions containing 15% MEG and varying concentrations of PEO-co-VP **40**
Fig. 3.8 Gas consumption (N) of 15% MEG and PEO-co-VP in varying concentrations **41**
Fig. 3.9 Onset time vs subcooling temperature of 1% KHI + 5% MEG, 1% KHI and the blank **45**
Fig. 3.10 (a) Onset time (t_{onset}), (b) growth time (Δt) and (c) percentage of gas consumption (N) of 1% KHI and 1% KHI + 5% MEG at 2.0, 5.2 and 8.0 °C **46**
Fig. 4.1 The onset times (t_{onset}) for 1% PEO-co-VP with MeOH in varying concentrations **49**
Fig. 4.2 The onset times (t_{onset}) for 0.5% PEO-co-VP and MeOH in varying concentrations **50**
Fig. 4.3 (a) The growth time (Δt) and (b) the percentage of consumption (N) for 1% PEO-co-VP and varying MeOH concentrations **51**
Fig. 4.4 (a) The growth time (Δt) and (b) the percentage of consumption (N) for 0.5% PEO-co-VP and varying MeOH concentrations **52**
Fig. 4.5 Hydrate conversion (ϕ) for 1% PEO-co-VP and MeOH in varying concentrations **53**
Fig. 4.6 Methanol molecule is incorporated into the water cage (obtained with permission from Shin et al., 2013) **54**
Fig. 4.7 PEO-co-VP concentration during hydrate growth in 0.5% PEO-co-VP + 15% MeOH solution **55**
Fig. 4.8 KHI concentration during hydrate formation in 0.5% KHI, 0.5% KHI + 15% MEG and 0.5% KHI +15% MeOH solutions **56**
Fig. 4.9 The effects of PEO-co-VP on the synergistic performance of (a) onset time (t_{onset}), (b) growth time (Δt) and (c) the percentage of gas consumption (N) in the presence of 10% MeOH **57**
Fig. 4.10 Hydrate conversion (Ø) for 10% MeOH with varying PEO-co-VP concentrations **58**

Fig. 4.11 Onset time versus subcooling temperature for 1% KHI + 5% MeOH, 1% KHI and the blank **60**
Fig. 4.12 Percentage of gas consumption (N) for 1% KHI and 1% KHI + 5% MeOH at various tested temperatures **61**
Fig. 4.13 Onset times for (a) 1% KHI + 5% MeOH and (b) 1% KHI + 5% MEG at various tested temperatures **62**

List of Tables

Table 2.1 Summary of hydrate formation at different agitation speeds **23**
Table 2.2 Onset temperature for mixed TIs and PEO-co-VP..... **24**
Table 3.1 Concentrations of KHI and MEG in the testing solutions (3.5% NaCl) ... **28**
Table 3.2 Hydrate formation with 1% PEO-co-VP at 2.0, 5.2, 8.0 and 9.8 °C..... **41**
Table 3.3 Hydrate formation with the blank at 2.0, 5.7, 9.0, 10.0 and 11.0 °C **43**
Table 4.1 Concentrations of KHI and MeOH in the test solutions (3.5% NaCl)..... **48**
Table 4.2 Hydrate formation with 1% KHI + 5% MeOH at 2.0, 3.0, 4.0 and 5.2 °C ...
..... **59**
Table 4.3 The value of ***a*** and ***b*** and the logarithm form of the fitted Arrhenius equation
..... **61**

Chapter 1 Introduction

1.1 Natural Gas Hydrates

Gas hydrates are clathrate compounds of small gas molecules encased in a cage-like structure of water molecules. Natural gas forms hydrates at high pressures and low temperatures, which are the common operation conditions for oil and gas production and transportation. The formation of gas hydrates is a continuous problem for the oil and gas industry because the hydrate particles may cause blockages that result in enormous pressure to the system, leading to irreparable damage such as pipeline ruptures (Luna-Ortiz et al., 2014). Resolutions normally involve complete shutdown of production, which often results in a huge economic loss. Besides the economic loss, hydrates blockages increase the risks to those who operate or maintain the production. The remediation is generally challenging because problems occur in unconventional locations (Giavarini and Hester, 2011). The likelihood of secondary incidents being introduced rises significantly when dealing with these problems (Daraboina et al., 2011). In 1992, a plugged pipe spool erupted from the ground due to hydrate-induced pressure and pushed aside the adjacent service truck, killing the foreman at this Chevron site in Canada (Koh and Creek, 2011). In addition, product spillages commonly are the consequence of such incidents, which raises environmental concerns.

Three different structures of hydrates have been discovered so far. These include structure I, II and H. The type of formed structures is largely dependant upon the size of the guest molecules. For instance, pure methane forms structure I (sI) hydrates at its equilibrium conditions. However, the presence of greater sized gases such as ethane and propane lead to the formation of structure II (sII) hydrates which is commonly seen in the natural gas production pipelines. As shown in Figure 1.1, the sI structure is made of cages that are pentagonal dodecahedrons and tetrakaidekahedrons, formed by water molecules through hydrogen bonding (Lederhos et al., 1996). Sharing the same small pentagonal dodecahedron cages as the sI, sII also contain bigger hexakaidecahedronal cages.

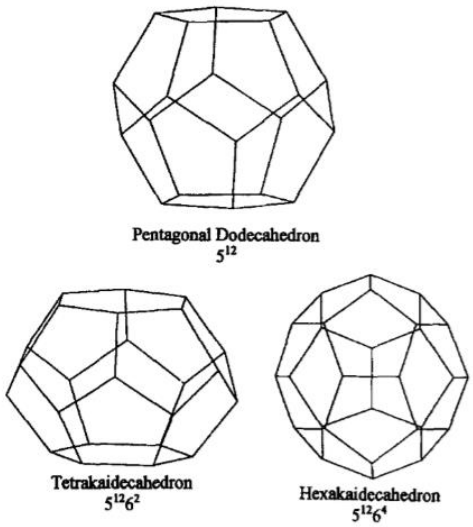

Fig. 1.1 Basic cages of sI and sII hydrates (Obtained with permission from Lederhos et al., 1996)

Hydrate formation kinetics has been widely investigated by laboratory researchers since the 1990s. It is well accepted that the formation of clathrate hydrates is similar to the crystallisation process that is initiated by nucleation of hydrates particles and is followed by the spontaneous growth of hydrates on a macroscopic scale, after reaching a critical particle size (Sloan and Fleyfel, 1991). The process can be either heterogeneous or homogeneous. Factors such as the solution chemical compositions, impurities interfaces and cooling conditions determine the actual formation conditions. In 1994, Sloan and his associate firstly explained the mechanism of hydrate nucleation with the labile cluster (Christiansen and Sloan, 1994). Within this work, The structure of the labile clusters is similar to sI and sII cages and they are formed by the water molecules arranging themselves around guest molecules. Local structuring was later proposed in 2002 by Radhakrishan and Trout, who suggested that the dissolved gas molecules drive the surrounding water molecules to form the cage-like structures (Radhakrishan and Trout, 2002). The most recent hypothesis, in 2010, was raised by Jacobson, combining the above two mechanisms through the presentation of amorphous clathrate (Jacobson et al., 2010). Within all the above hypotheses, the growth of hydrate particles into clusters of a critical size is fundamental to the formation of the hydrate.

1.2 Chemical Inhibition of Natural Gas Hydrates

Chemical injection is widely used in the industry for the prevention of hydrate formation in the field. The most effective and commonly used chemicals include monoethylene glycol (MEG) and methanol, which are classified as thermodynamic inhibitors (TIs). Low dosage hydrate inhibitors (LDHIs) including the kinetic inhibitors (KHIs) and the anti-agglomerants (AAs) have attracted increasing attention in the past two decades. The classification of the chemicals is based on their mechanisms of interaction.

1.2.1 Thermodynamic inhibitors (TIs)

Thermodynamic inhibitors shift hydrate formation equilibrium to a lower temperature and higher pressure through hydrogen bonding with water molecules. The performance of the TIs is proportional to their concentrations in the liquid phase. This can be explained using MeOH as an example. Shown in Figure 1.2 are the thermodynamic equilibrium curves, predicted using CSMGem, of the methane gas hydrates in the presence of 0%, 5%, 10%, and 20% MeOH, respectively, by weight (Lafond et al., 2012). For each curve, the hydrate-free region is on the right side of the curve and hydrates tend to form on the left. As MeOH concentration is increased, these curves move further to the left, allowing the hydrate-free zone to extend to a lower temperature and higher pressure. For example, at the given system operating pressure of 150 bar, the formation temperature reduces from over 13°C to less than 5 °C when MeOH concentration increases from 0 to 20%.

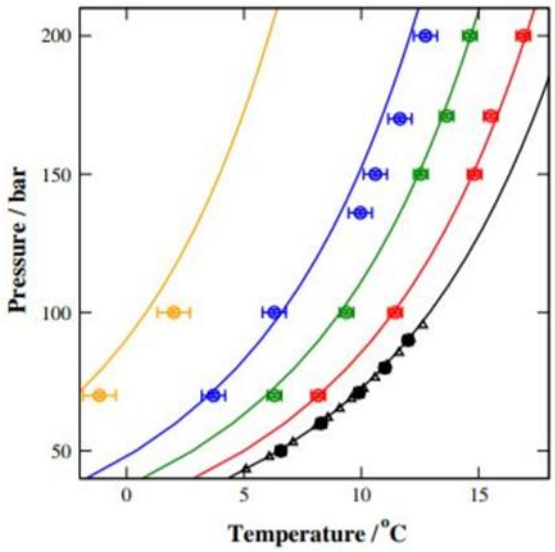

Fig. 1.2 Methane gas hydrate equilibrium curves with methanol concentrations of 0wt% (red), 0.05wt% (green), 0.10wt% (blue) and 0.20wt% (orange) in a 3.5wt% sodium chloride solution (predicted by GSMGem) (Obtained with permission from Lafond et al., 2012)

For field applications, the selection of a TI is based on a balanced consideration of factors such as field conditions, capital expenditure on transportation storage facilities (CAPEX), operational expenditure (OPEX), material accessibility and safety (Luna-Ortiz et al., 2014). Both MeOH and MEG are the most popular TIs in the field because of economic and availability considerations. MeOH was reported to provide reliable inhibition under high subcooling conditions. However, with the increasing awareness of safety and environmental concerns, additional cost is required for the removal of MeOH from any liquid carbon that contains a high concentration of MeOH (Kidnay and Parrish, 2006). In addition, MeOH is restricted in its use for offshore drilling because it is classified as a highly toxic substance to both the environment and people (Talaghat, 2014; Brustad et al., 2005). MEG is considered to be the preferable TI according to health, safety and environmental (HSE) issues (Cha et al., 2013a). Furthermore, the regenerated MEG can be directly recycled in the production process after the simple evaporation of water. On the other hand, the use of MEG increases the liquid phase viscosity, adding to the OPEX due to the increased transportation cost. Local accessibility is another factor to be considered for the selection of TIs. For example, ethanol is widely used in South America because it is available in large

quantities from sugar fermentation (Kelland, 2014). Furthermore, inorganic salt such as sodium chloride also demonstrates the property of being a thermodynamic inhibitor.

1.2.2 Low dosage hydrate inhibitors (LHDIs)

Although TIs are very effective in most field applications, hydrates inhibition with TIs requires substantial investments, usually up to 10-15% of the production cost, with typical usage of 40-60% by weight (Brustad et al., 2005; Kelland, 2014). With growing environmental awareness, researchers started to look for alternative hydrate inhibitors requiring lower dosage. Since the 1990s, low dosage hydrate inhibitors (LDHIs) have been introduced to industrial practice with the effective concentration being below 1%. These new inhibitors are even more appealing to new plants, due to a reduction in the size of the facility, including storage, pumping station and pipeline. LHDIs are further divided into kinetic hydrate inhibitors (KHIs) and anti-agglomerants (AAs) according to their behaviour during hydrate formation. Owing to surfactant properties, both AAs and KHIs have been reported mainly on the interface during hydrate formation; however, their working mechanisms are different (Leporcher et al., 1998).

AAs are surfactants that effectively prevent the hydrate particles' agglomeration rather than their formation. They are mainly applied in oil production with the maximum water-cut of 50% (Peytavy et al., 2008). In the presence of an AA, the oil phase is considered as the carrier of hydrate particles so that the hydrates form a slurry-like fluid and become transportable (Moradpour et al., 2011; Zare et al., 2015). The performance of AAs can be expressed to their resistance to the tendency of the hydrate to plug the pipeline (plugging potential) (Sharifi and Englezos, 2015). AAs have been reported to be very effective at high subcooling temperatures or for shut-in conditions (York and Firoozabadi, 2008). According to Kelland (2006), single-tailed quaternary AAs appear to be the only type of LDHI that can constantly perform when subcooled at 15 °C or more (Kelland, 2006). In contrast, KHIs mainly work on gas production and have been used in the upstream oil and gas industry for over two decades (Del Villano and Kelland, 2011). They are generally polymeric compounds and have been found to delay nucleation and decrease growth rate (Christiansen and Sloan, 1994; Lederhos et al., 1996). KHIs work well in the field with limited subcooling of around 12 °C (Patel and Russum, 2010; Perrin et al., 2013). Biological substances, including

antifreeze proteins known as AFPs, are also regarded as kinetic hydrate inhibitors (Sharifi and Englezos, 2015).

Different from AAs, KHIs affect both the nucleation and growth stages (Kelland et al., 1995). KHIs interact with local water clusters to increase the barrier of nucleation, so that less water molecules form hydrate cages and critical nucleation is hindered (Daraboina et al., 2015). Without direct evidence of the nucleation inhibition mechanism, inhibition of the growth stage is studied to provide supplementary information to explain the overall inhibition mechanism. During the growth stage, the active functional groups of KHIs attach to the crystal surface, and ongoing crystallisation of the hydrate is then forced to follow certain patterns around/between the polymer strands (Luna-Ortiz et al., 2014). Makogon reported that the adsorption of the polymer side group onto the hydrate surface through hydrogen bonding blocks the gas molecules from entering the hydrate cavity (Makogon et al., 2000). Del Villano and Kelland (2010) suggested that the polymeric inhibitor was embedded in the hydrate surface through the penetration of one branch alkyl group into the open cavity. Therefore, water molecules re-arranged themselves around the rest of the hydrophobic side polymer chains and, thus, the growth was hindered (Del Villano and Kelland, 2010). Gas hydrates form at the water-gas interface and act like a barrier that reduces contact between the bulk liquid and the gas phase (Semenov et al., 2015). Therefore, further hydrate growth is kinetically controlled by this hydrate layer, including its morphological properties after nucleation (Sharifi and Englezos, 2015). The attractive force between the side group and the hydrate surface has been believed to be the reason for the adsorption to inhibit hydrate formation. However, the range of the attractive force is sub-nanoscale, implying that this force has no effect on the macroscopic mass transfer of guest molecules in the crystal growth processes of gas hydrates (Yagasaki et al., 2015).

Despite the inhibition effect during hydrate growth, KHIs have been reported to have a promotional effect on the growth. Catastrophic growth has been proposed as an elaboration of the promotion effect, owing to the hydrate morphology that facilitates capillary movement of water molecules to the gas/liquid interface (Sharifi and Englezos, 2015). During growth, porous hydrate layers have been observed at the liquid-gas interface instead of a non-porous film in the presence of KHIs in quiescent

systems. More water molecules are then drawn up to form hydrates rather than being blocked from further growth (Verrett et al., 2012). The growth also can be viewed from the increased level of gas molecules. The carbon backbone present in KHIs has little effect on the solubility of methane during nucleation. However, it can increase the methane mole fraction in the liquid phase during the hydrate growth period (Mokhatab et al., 2007). This further confirms that the interface between hydrate particle and liquid may be the controlling factor of hydrate growth, not the interface between solid and gas.

In the laboratory, hydrate formation in the presence of KHIs can be tested over time using different apparatus including a rotation rig, high pressure cell and flow loop (Arjmandi et al., 2002; Del Villano et al., 2009; Lederhos et al., 1996). The pressure and temperature changes with time can be directly collected to reflect the hydrate formation kinetics. Parameters derived from these data are then used to quantify the inhibitor performance in the targeted stages including onset time, growth time, gas consumption, onset temperature, growth rate and subcooling temperature. Among all these parameters, onset time and subcooling temperature are the most frequently used criteria for determining the effectiveness of KHIs because they directly reflect the field conditions. (Kelland et al., 2015; Kim et al., 2018)

Onset time is commonly reported to represent the time point when the hydrate is first detectable, and it correlates to the nucleation inhibition (Kashchiev and Firoozabadi, 2003). Subcooling is defined as the temperature difference between the operation and the equilibrium of the given operating pressure (Arjmandi et al., 2005). It also represents the driving force, and is inversely proportional to hydrate onset time. The more powerful the inhibitor, the greater the level of subcooling it can withstand over a longer period.

1.3 Synergists to the Inhibition Performance of KHIs

It is well accepted that the effectiveness of KHIs is sensitive to temperature. KHIs are unlikely to work alone in the field to provide sufficient inhibition in situations of high subcooling temperature (Perrin et al., 2013). Many substances have been found to boost KHIs' performances, along with the innovation of new KHIs. This group of materials is named as 'synergists'. Synergists do not show inhibition of hydrate

formation but can improve the performance of LDHIs when working together (Daraboina et al., 2013a). In 1996, the first synergistic effect was reported when Tetra-n-butylammonium bromide (TBAB) was used together with polyvinylcaprolactam (PVCap) (Nakarit et al., 2013). The effect of TBAB was later classified as causing anti-agglomeration. Other chemicals such as ionic liquid, inorganic salt, oxides, quaternary ammonium salts and phosphonium salts, and glycol ether have been reported to strengthen LDHIs' inhibition performance (Cha et al., 2013a; Zare et al., 2015; York and Firoozabadi, 2008; Del Villano and Kelland, 2010; Li et al., 2010; Szymczak et al., 2006; Sun et al., 2012; Ke et al., 2013; Cohen et al., 1998; Huo et al, 2014; Tariq et al., 2014; Ding et al., 2010; Kim et al., 2014; Magnusson and Kelland, 2014). However, their application remains limited due to the uncertainty of the working mechanism. In fact, most synergists show similar properties to thermodynamic inhibitors when they are tested alone. Currently, TIs are easily accessible and still considered as the most reliable source. The application of KHIs is able to utilise the existing facility.

A common practice utilising the TI/KHI synergistic effect is when the expected subcooling in the field is higher than that of the existing KHI. TIs are then injected to shift the hydrate formation equilibrium to the region of lower temperature and higher pressure. By doing so, the degree of subcooling is reduced to the range for which KHIs are suitable (Tohidi et al., 2014). Another application of the synergistic effect is to significantly reduce the amounts of TIs required by using a marginal quantity of LDHIs (Tohidi et al., 2014). This leads to the reduction of costs associated with storage and transportation.

The first research on the synergist effect between KHIs and TIs was reported in 1998. Cohen *et al* (1998) reported that the inhibition performance of mixtures of poly(vinyl caprolactam) and vinyl caprolactam/vinylpyrrolidone was significantly improved by adding 2-butoxyethanol. This solvent is still widely used in the oilfield today to improve the effect of KHIs on hydrate inhibition; however, the underlying mechanism remains unclear (Perrin et al., 2013). Since then, much research has been carried out to improve the LHDIs' effect through adding various TIs as solvents and leading to more effective inhibition. Low carbon alcohols have been found to greatly enhance the inhibition performance of both KHIs and AAs. Their performance in improving the

action of LDHIs is generally evaluated using the subcooling temperature, the onset time, the inhibitor dosage and the hydrate volume fractions (Kim et al., 2014; Kelland, 2006; Talaghat, 2013).

More systematic research has been conducted in the laboratory to investigate the performance of various TIs in strengthening the actions of LHDIs. Kim *et al* (2014) tested KHI enhancement by MEG with relatively high concentrations of 20% and 30% on natural gas hydrate inhibition. They claimed that glycols promoted the performance of KHIs by postponing onset time, thus hindering the growth of crystal particles. In both MEG concentrations, the mixtures containing 0.2wt% PVCap reduced the hydrate volume fraction from 0.77 and 0.66 to 0.29 and 0.15, respectively. It has been demonstrated that hydrate slurries with a volume fraction varying from 0.1 to 0.3 are transportable inside pipe work while in liquid phase (Akhafash et al., 2013). Besides, the hydrate formed with 30wt% MEG concentration is structure II hydrate, whereby metastable structural I hydrate has been suppressed to structure II. Cha *et al* (2013a) also reported the synergistic effect on natural gas hydrate inhibition between polyvinyl pyrrolidine (PVP) and MEG, with the onset time for PVP being extended from 26.6 to 85 minutes with 30wt% MEG. The molecular simulation illustrated that, when PVP moves to the interface of water and methane, it forms a membrane to stop further hydrate nucleation (Kuznetsova et al., 2010). MEG helps PVP with its adsorption to the hydrate surface to stop methane enter the water cage cavities.

Traditionally, thermodynamic inhibitors are used where high subcooling is required. With the aid of TIs, the subcooling of operational systems that were controlled by a KHI increased. Huo *et al* (2014) reported that the addition of 0.8 wt% PVCap made the subcooling temperature increase from 11.1 to 15.18 °C when methanol concentration rose from 5 to 15 wt%. The increased subcooling by the solvent breaks the KHIs' operation limit of 12 °C, and further extends their utilisation into harsh environments where sites operate under even lower temperatures and/or higher system pressures (Patel and Russum, 2010; Perrin et al., 2013). Yet, the correlation between solvent and KHIs to achieve optimised result has been less studied.

Studies of both commercially available and custom-designed new KHIs conducted by our group have shown an apparent synergistic effect of the KHIs with low carbon

alcohols including methanol, ethanol and MEG (Ding et al., 2010; Lou et al., 2012). Our recent study on the effect of mixtures of PEO-co-VCap-1 with MEG, MeOH and ethanol on the inhibition of tetrahydrofuran (THF) hydrates further revealed that the synergistic effect was a result of adsorption of the KHI polymers onto the THF hydrates (Foo et al., 2016). A strong correlation between the KHI concentration and inhibition performance was reported in this work. Although THF hydrates share the sII structure with the natural gas hydrates, THF is hydrophilic, while methane gas hydrates are hydrophobic (Perrin et al., 2013). Extended work involving natural gas hydrates is required for an in-depth understanding of the inhibition of methane hydrates by the synergistic effects of TIs with such KHIs.

In recent years, significant amounts of work on hydrate inhibition strategies have shifted to the understanding and application of inhibition systems involving both KHIs and TIs (Kim et al., 2014; Tohidi et al., 2014; Mozaffar et al., 2016; Zhao et al., 2015; Foo et al., 2016; Qin et al., 2016; Kim et al., 2017). The work is especially appealing in field applications because fewer modifications are required on the existing production infrastructure. In addition, it meets the harsh production requirement where the need for subcooling is high. The mechanism of the synergistic effect has been investigated through correlating the synergistic inhibition performance with various parameters, including polymer concentrations, interfacial tensions, torque value of agitation and morphological observations. However, the hypotheses that have been proposed by different groups still require further direct evidences to support them. Besides, research on the inhibition of TIs and KHIs is not only limited to the sII hydrate but also has focused on the sI hydrate structure (Kim et al., 2017).

1.4 Scope of Work

The purpose of this thesis is to investigate the synergistic effect of MEG and methanol on the inhibition performance of a new KHI made of copolymers of poly(ethylene glycol) methyl ether methacrylate (PEOMA) and vinyl pyrrolidine (VP). The overall objectives of the project are:

- To investigate the kinetic inhibition performance of the KHI towards the natural gas hydrates;

- To study the synergistic effect of MEG and MeOH in combination with the KHI;
- To assess the concentration- and temperature-dependence of the inhibition performance and the synergistic effects; and
- To obtain further understanding of the underlying mechanisms of the synergistic effects.

Details of the research methodology, the experimental set-up, the testing formulae and the experimental parameters that were determined will be provided in the following chapters.

Chapter 2 Experimental Set-up and Procedures

2.1 Introduction

This chapter reports the experimental set-up and procedures that were developed for the required experimental work. All hydrate formation experiments were carried out in a sapphire high pressure cell (200 ml). Experimental conditions including temperature, pressure and agitation speed were first determined using a 3.5 wt% sodium chloride solution and the synthetic natural gas in the reactor. Changes in pressure and temperature with time were directly measured during hydrate-forming experiments. Other parameters, such as onset time, growth time, percentage of gas consumed and percentage of hydrate converted, were determined based on the collected experimental data. Ultraviolet-visible spectroscopy (UV-Vis) was used to detect the KHI concentrations during the formation process of the hydrates. The details will also be discussed in this chapter.

2.2 Chemicals and Materials

MEG (Chem-Supply, >99%), MeOH (Sigma-Aldrich, > 99.9%) and sodium chloride (Lab-Scan Analytical Science, 99%) were purchased and used as-received. All chemicals were analytical reagent (AR) grade. Deionised water was used in all experiments.

Synthetic natural gas (SNG) consisting of methane, ethane and propane in the molar ratios of 93:5:2, respectively, was supplied by BOC Australia. Poly(ethylene oxide-co-vinylpyrrolidone) (PEO-co-VP) (Fig. 2.1) was used as the kinetic inhibitor in this study and was provided in-house.

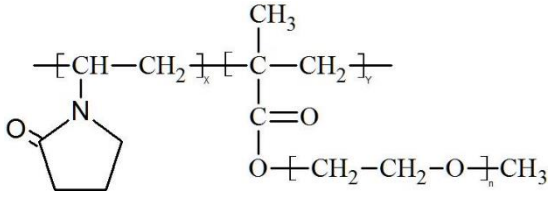

Fig. 2.1 Chemical structure of PEO-co-VP

Hydrate-forming solutions were prepared by mixing PEO-co-VP and the selected TI in the sodium chloride solution (3.5%) according to a previously reported method (Ding et al., 2010; Foo et al., 2016). Sodium chloride solution (3.5 %) was made by dissolving 35 g of sodium chloride in 965 g of water. This solution was then filtered and stored under ambient conditions. The percentage concentration was weight-based and is used throughout the thesis unless it is specifically stated otherwise. More details of the chemical compositions of the hydrate-forming solutions will be provided in Chapters 3 and 4.

2.3 Experimental Set-up

2.3.1 High pressure cell

The sapphire high pressure cell (Top Industries High Pressure Engineering, France) that was used for this study is of cylindrical shape with an internal volume of 200 ml (Fig. 2.2②). The internal diameter and height are 50 and 100 mm, respectively. It was designed to withstand pressures up to 20 MPa and temperatures in the range of -20 to 50 ºC. A liquid sampling compartment was designed involving two valves that allow a maximum volume of 1ml of liquid sample to be removed in one operation (Fig. 2.2③). A data acquisition system (DAQ) (Fig. 2.2④) was connected to the high pressure cell and supplied by the same supplier. The system was also connected to two temperature sensors (PT100, FICH) and one pressure sensor (SY23, Keller). One temperature sensor was housed in the thermowell mounted on the top of the high pressure cell to measure the temperature of the gas phase, and the other was positioned in the bottom of the cell for measuring the liquid phase, with a resolution of ±0.1 ºC (Fig. 2.2⑥). The pressure sensor was placed in the gas phase and measured with an accuracy of ±0.01 MPa (Fig. 2.2⑦). An H-anchor paddle stirrer was coupled with a magnetic motor for agitation in the centre of the cell (Fig. 2.2⑤). The maximum speed of this stirrer is 2,000 rpm. Temperature, pressure and speed of stirrer could be recorded at intervals ranging from 1 to 60 seconds. During hydrate formation, all data were collected at the interval of 5 seconds. A schematic diagram of the high pressure cell and its accessories is presented in Figure 2.2.

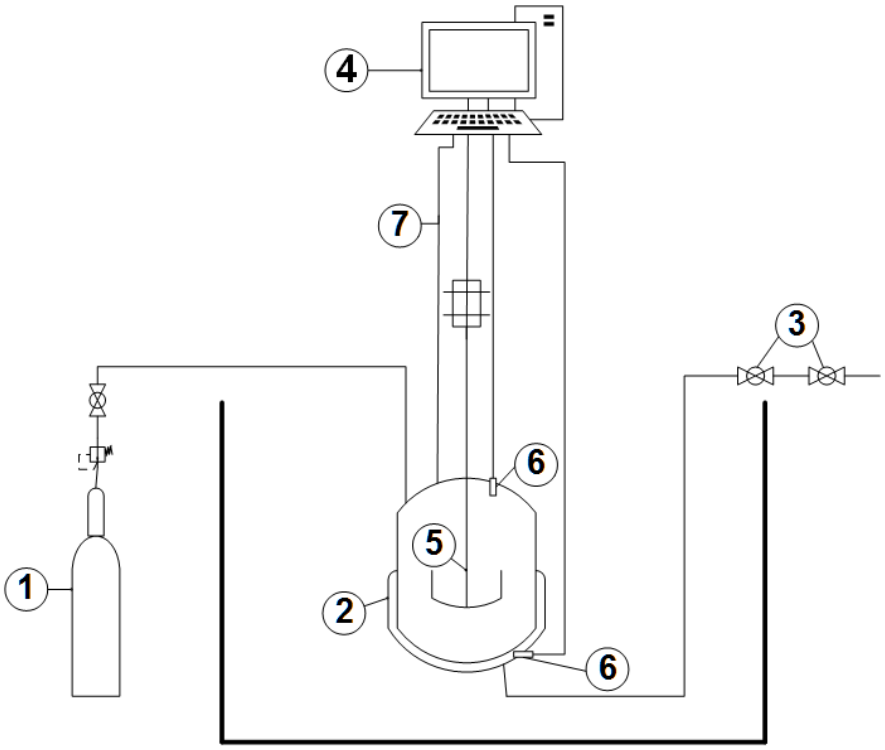

Fig. 2.2 Schematic diagram of the high pressure cell with its accessories

①Gas bottle, ② High pressure cell, ③ Sampling valves, ④ Controller (DAQ), ⑤ Stirrer, ⑥ Temperature sensors, ⑦ Pressure sensor

2.3.2 Temperature control bath

A temperature control bath was used to achieve and to maintain the required temperature of the high pressure cell (Fig. 2.3). The bath (Fig. 2.3①) was designed to hold up to 80 L of coolant and was filled with a mixture of ethylene glycol (20 L) and water (60 L). The bath was controlled by a separate LabVIEW program through a DAQ system (National Instrument). This program provided the communication between the controller and other hardware (Fig. 2.3⑥). A coiled immersion probe formed a cooler (1/4HP, IP 40, PolyScience) and was employed to chill the liquid in the bath (Fig. 2.3②). A coiled heater (1.25 kW, SPI, Electric Elements) was used to generate heat to compensate for the cooling (Fig. 2.3③). The cooler ran constantly during the operation. The heater was operated by the controller through an on/off relay (Fig. 2.3⑤). The temperature of the bath was detected by an RTD-type temperature sensor that was provided by the same supplier (Fig. 2.3④). The coolant was circulated

using a static coolant pump (10.5 m^3/hr, AquaPro) (Fig. 2.3⑦). The lowest achievable temperature for the bath was -12.5 °C.

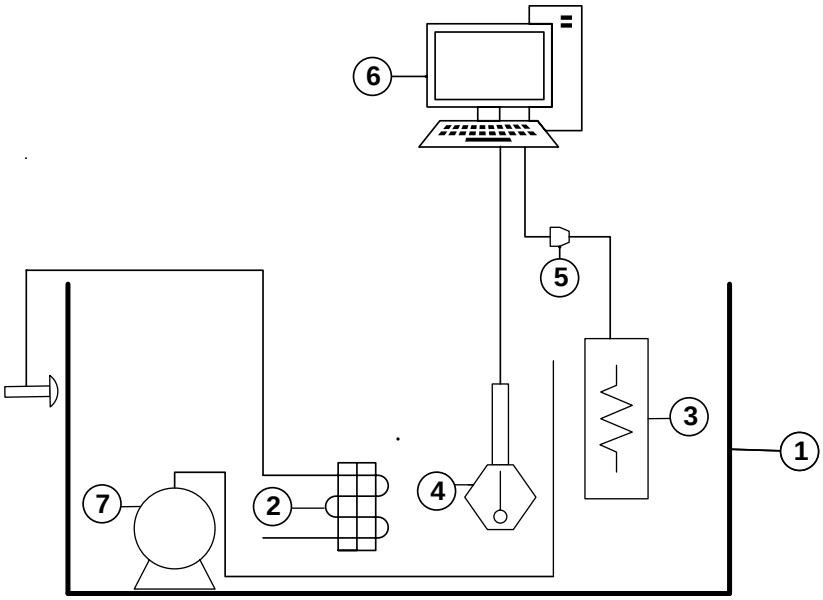

Fig. 2.3 Schematic diagram of temperature control bath

① Bath, ② Cooler, ③ Heater, ④ Temperature sensor, ⑤ On/off relay, ⑥ Controller (DAQ), ⑦ Coolant pump

Other components included a gas release valve (1/16", Type 4) and a rupture disc pressure relief valve (1/4", BSP) that protected the system from being over-pressurised (Fig. 2.4). All tubing was supplied by Top Industries and was fabricated in C276 material. The complete reactor set-up is displayed in Figure 2.4.

Fig. 2.4 Complete assembly of experiment apparatus

2.4 Experimental Procedures

The hydrate formation procedure was modified from the reported work of Sharifi and Englezos (2015). For each hydrate formation experiment, 30 ml of testing solution was injected into the high pressure cell. The cell was then sealed and purged twice with the synthetic gas to remove the residual air. During each purging, the cell was kept at the purging pressure of above 3 MPa for 5 min to ensure no leakage was detected. Meanwhile, the stirrer was set to 600 rpm to help the solution to become saturated with SNG gas, thus the residual air was removed to the maximum extent.

Once the cell had been prepared, the temperature and pressure of the high pressure cell were adjusted to 18 °C and 7 MPa, respectively, and maintained at this condition for 15 min. The cell was then cooled to the pre-set temperature (2 °C) and kept at this temperature for 15 min. At this temperature, the ice-induced hydrate nucleation could be avoided (Staykova et al., 2003). The stirrer was then started at the speed of 600 rpm. The corresponding time was marked as time zero (t_{zero}) and regarded as the start of each reaction. This condition was then maintained for the rest of the reaction. For repeated experiments, the cell was heated to 18 °C within 3 h and held at this temperature for at least 6 h prior to the commencement of the next run.

During each reaction, T, P and t were directly recorded at intervals of 5 sec. Figure 2.5 shows a typical P-T-t curve with the hydrate-forming solution containing 1% PEO-co-VP. The onset time (t_{onset}) and the time at the completion of hydrate formation (t_{end}) were determined by the pressure change. The time point at which hydrate was first detected, t_{onset}, was used to quantify the nucleation time. Since the direct observation of nucleation was impossible, t_{onset} and t_{end} were correlated to the times at which the pressure drop exceeded 0.01 MPa in the period of 5 and 15 min, respectively. As shown in Figure 2.5, the onset of hydrate formation is accompanied by a sharp pressure drop (red line) and a temperature rise in the gas phase (blue line). It should be noted that the temperature peak was not always visible in this study. However, the pressure drop appeared in all experiments where hydrates formed. Therefore, the reported onset time in this thesis work was determined using the time at which the pressure drop exceeded 0.01 MP within 5 min. The subcooling temperature, which is the difference between the pre-set and thermodynamic equilibrium temperatures, was computed

under the same condition (Tohidi et al., 2012). The equilibrium temperature was calculated with CSMGem using the specified gas composition in all experiments.

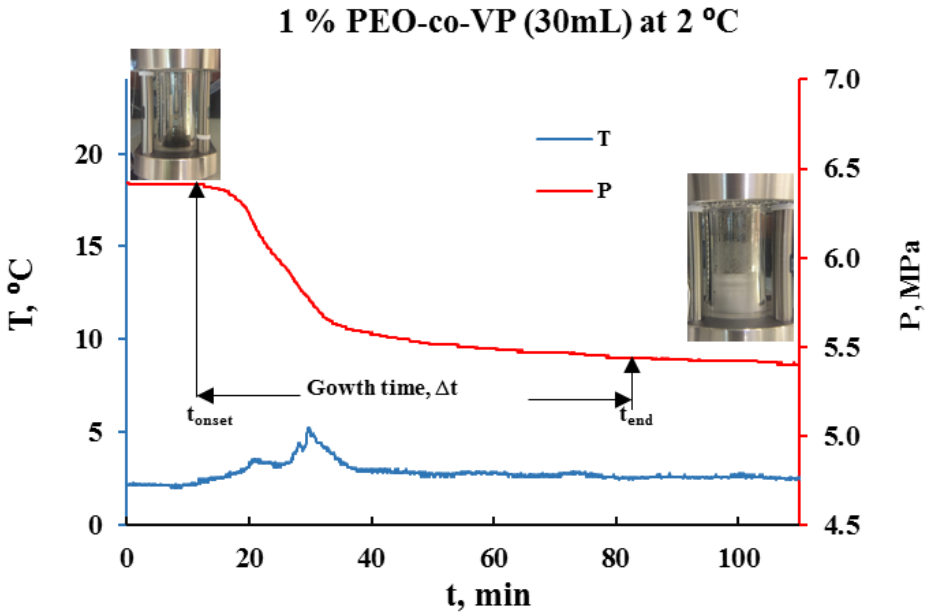

Fig. 2.5 Pressure-temperature-time (P-T-t) curves of the hydrate-forming solution containing 1% KHI

The growth time (Δt) was acquired from the time difference between the completion (t_{end}) and onset (t_{onset}). A longer growth time indicated a slower growth rate. The growth time was used to describe the growth kinetics beyond the initial nucleation (Englezos, 1993). To compare the growth rates, time points of t_{40} and t_{80} were used in this study. They refer to the times at which the formed hydrates reached 40% and 80% in respect to the theoretical amount of hydrates.

Onset temperature (T_{onset}) was also determined in some experiments. It was examined in order to select the pre-set temperature (T_{set}) that correlate to the greatest sub-cooling temperature. The onset time (t_{onset}) were then measured under a same T_{set} and used to evaluate inhibition performance. In brief: the high pressure cell was first prepared as previously detailed. The high pressure cell was rapidly cooled from 18 °C to 6 °C (this temperature is about 2 °C above the equilibrium temperature of all hydrates forming systems) within 4 h the maximum capacity of the chiller while the stirrer was kept running at 600 rpm. A further reduction of temperature was achieved by controlling the cooling rate at 1 °C/hr. Therefore, the effect of cooling rate on the onset temperature

was considered the same for all systems. The temperature at which the formation of hydrates was first detected was regarded as the onset temperature (T_{onset}). As shown in Figure 2.6, the detection of hydrate onset was determined by the pressure drop exceeding 0.01 MPa within 5 min. The temperature that corresponded to the onset was taken as onset temperature (T_{onset}). Visual observations of hydrates and temperature spikes in the liquid phase were generally consistent with the pressure drops. However, a temperature spike was not observed in all experiments.

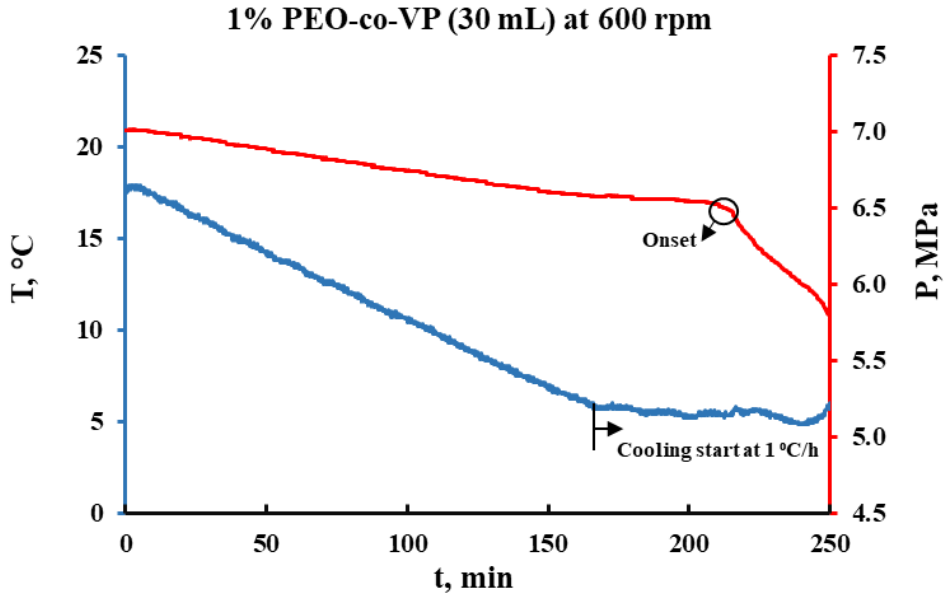

Fig. 2.6 Determination of the onset temperature from the P-T-t curve of the hydrate-forming solution containing 1% KHI at 600 rpm

2.5 Sample Extraction

For some experiments, liquid samples were extracted from the high pressure cell at the beginning of the agitation, at the onset time and at other pre-determined times. As shown in Figure 2.2, two identical valves that were connected by a piece of pipe were installed in the sampling line. During the process, the valve next to the high pressure cell was opened first, to allow the sample to move into the pipe section, and was then shut off. The liquid was then released to a pre-weighed sampling bottle. The liquid sample and the bottle were weighed again to yield the total weight of sample collected. The time for sampling was selected according to the length of the reaction. The intervals between sampling times ranged from 20 to 30 min after the onset of hydrate

formation. The extracted samples were diluted using the stock solution for further analysis using a UV-Visible spectroscope. Details will be described in Section 2.8.

2.6 Gas Consumption Calculation

The total moles of gas (n_{total}) consumed during the hydrate formation experiment was calculated using equation (1), where the pressure (P) and temperature (T) can be obtained from the experimental P-T-t curve. V is the volume of gas, which is the volume of the high pressure cell subtracted from the volume of charged solution (assuming no volume change resulted due to the conversion of liquid to solid), and z represents the compressibility factor, calculated using the Peng Robinson equation of state (EOS) (Lopez-Echeverry et al., 2017). Subscripts i, and c denote the conditions at initiation and completion of the reaction, respectively. R is the gas constant.

$$n_{total} = \frac{P_i V}{z_i R T_i} - \frac{P_c V}{z_C R T_C} \quad (1)$$

Similarly, the moles of gas consumed at time t (n_t) can be calculated with equation (2). The subscripted t denotes the time t.

$$n_t = \frac{P_i V}{z_i R T_i} - \frac{P_t V}{z_t R T_t} \quad (2)$$

The percentage of hydrate formation (ϕ) then can be defined with n_t and n_{total} using equation (3).

$$\phi = \frac{n_t}{n_{total}} \times 100\% \quad (3)$$

The percentage of gas consumption (N) is calculated with equation (4).

$$N = \frac{n_{total}}{n_T} \times 100\% \quad (4)$$

Thus, n_T is the moles of gas required to convert all water into hydrates (theoretical calculation). In each reaction, 30 ml of 3.5% sodium chloride solution was used to

form the hydrate. Approximately 0.57 moles of gases were charged into the reactor, which is in excess of the water. Assuming that the hydration number in hydrates is 6.5 (Park et al., 2016), the theoretical moles of gas (n_T) required to convert water to hydrate can be calculated by equation (5), where ρ_w and M_{H_2O} are the molar density and mass of water, respectively.

$$n_T = \frac{30\ X\ 96.5\%/\rho_w}{(M_{H_2O} \times 6.5)} \qquad (5)$$

2.7 Experimental Conditions

2.7.1 Agitation speed

Hydrate formation is limited by mass transfer. Sufficient agitation is required to create effective contact between gas and water molecules in order to reach a high yield. Proper agitation speed also ensures the reproducibility of the results. In this work, four different speeds were examined. These included 200, 400, 600 and 800 rpm. All reactions were conducted with 30 ml deionised water and under the pre-set temperature of 2 °C. The P-t, T-t and n_t-t curves are shown in Figure 2.7. Hydrate formation was observed immediately after agitation started in all cases. The apparent pressure drop (Fig. 2.7a) and the temperature rise (Fig. 2.7b) were observed during the formation of hydrates at 400 rpm, 600 rpm and 800 rpm. No significant change in the pressure and temperature was demonstrated up to 120 min when the agitation speed was 200 rpm, indicating a very slow formation process. This could be a result of the low speed being insufficient to mix the liquid-gas phases in the reactor, preventing the further growth/formation of gas hydrates. Figure 2.8 shows a thin layer of hydrates that formed on the top of the liquid phase, which was stable and grew thicker up to the period of 120 min. (Hydrate onset was observed immediately after agitation.)

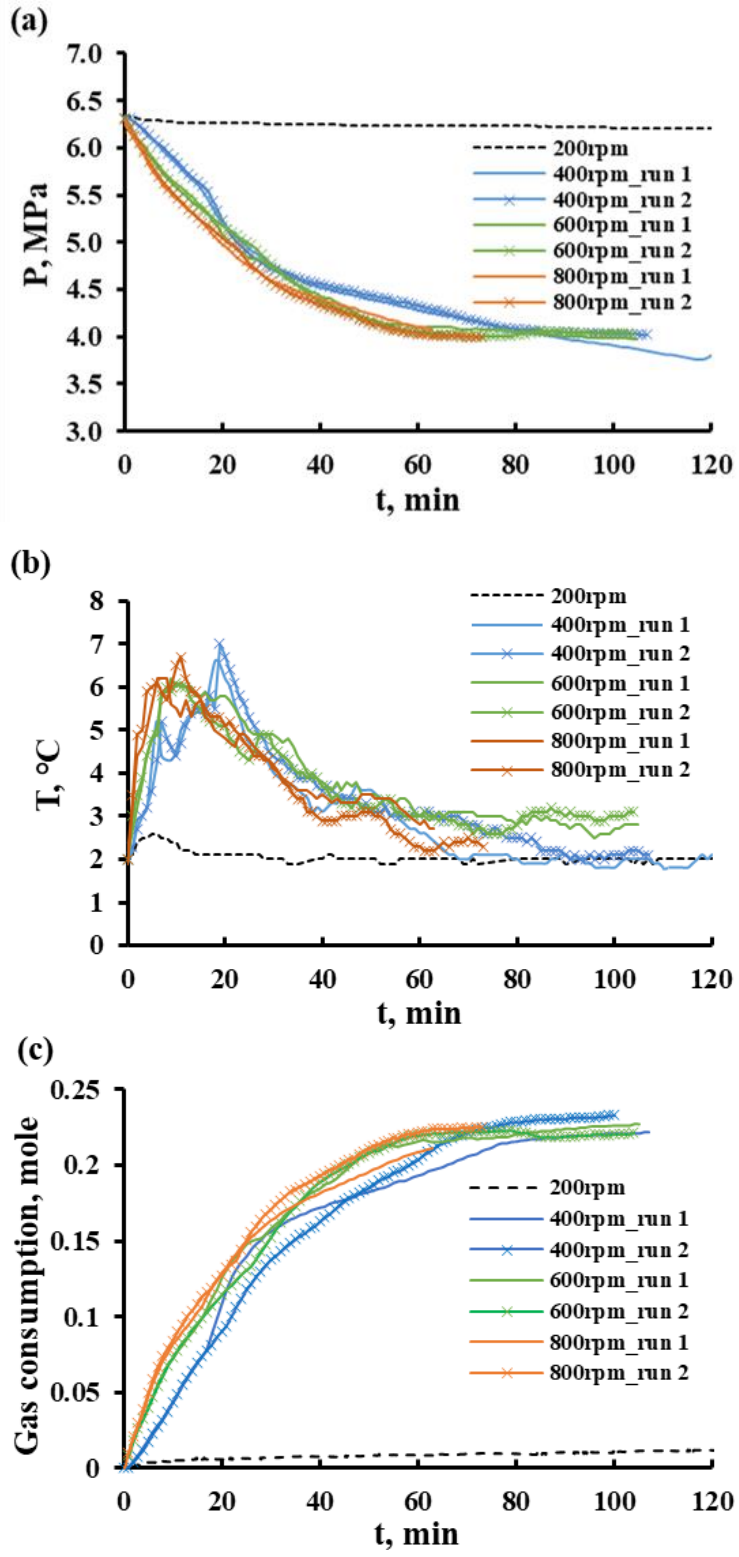

Fig. 2.7 The time profiles of (a) pressure (P), (b) temperature (T), and (c) gas consumption in deionised water (30 ml) at various agitation speeds

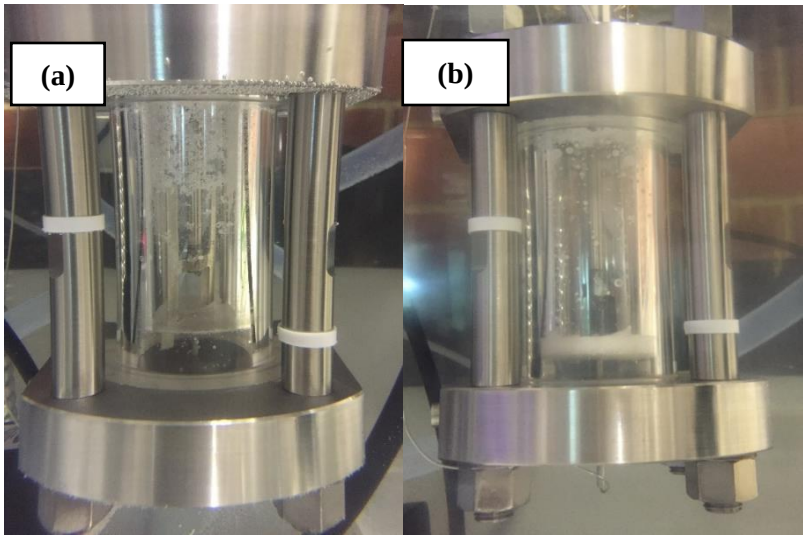

Fig. 2.8 Photographs showing hydrate formation at onset (a) and at 120 min after onset (b) at 200 rpm (30 mL DI water, T=2.0 °C, P=6.33 MPa)

For each successful agitation speed (400, 600 and 800 rpm), two repeated experiments were conducted. Within the investigated time frame, the calculated percentage of gas consumption and the growth time are presented in Table 2.1. With increased agitation speed, the growth time was decreased as a result of increased reaction speed. However, the percentage of gas consumption was reduced. This is due to the increased mass transfer restriction, according to the level of agitation. In general, the range of reaction speeds and gas consumption was feasible for the study. Finally, the speed of 600 rpm was selected for the thesis study because the results were more consistent over the two repeated experiments.

Table 2.1 Summary of hydrate formation at different agitation speeds

Agitation Speed, rpm	Growth Time, min	Percentage of Gas Consumed, %
400	126	91
	107	87
600	105	89
	100	86
800	63	82
	73	88

2.7.2 Onset temperature

The onset temperatures of various hydrate-forming solutions were tested according to the procedure detailed in Section 2.4. The results are summarised in Table 2.2. It is apparent that, at a constant KHI concentration, increasing MEG or MeOH could reduce the onset temperature. Similarly, at a constant TI concentration, increased KHI concentration has resulted in a decrease in onset temperature. For the thesis work, 2 °C was selected as the pre-set working temperature to determine the onset time. This should ensure sufficient driving force and a practical onset time to be monitored while avoiding ice-induced nucleation.

Table 2.2 Onset temperature for mixed TIs and PEO-co-VP

PEO-co-VP, %	TI, %	Onset Temperature, °C
	MEG, 0	5.4
	MEG, 10	0
	MEG, 15	-6.8
	MeOH, 5	3.0
0	MeOH, 10	-2.0
	MEG, 15	1.4
0.75	MeOH, 10	-1.9
	MEG, 15	0.2
0.5	MeOH, 10	4.3
0.25	MEG, 15	3.0
	MEG, 15	4.3
0	MeOH, 10	1.9

2.8 UV-Vis Spectroscopy

In this work, UV-Vis spectroscopy (Lambda 25) was used to determine the KHI concentration of liquid samples that were extracted from the high pressure cell, according to our previously reported method (Foo et al., 2016). The change in the KHI concentration directly supports the inhibition mechanism that has been speculated about in the past, which can be attributed to either the physical adsorption of KHI on the hydrate surface or perturbation of the remaining liquid phase (Kelland et al., 2012). Previously, our group reported that the PEO-co-VCap-1 concentration decreased in the liquid phase during THF hydrate growth. The adsorption of PEO-co-VCap-1 on the hydrate surface was hypothesised to be responsible for the decrease in KHI concentration (Foo et al., 2016). The PEO-co-VP has a similar structure to PEO-co-VCap-1, with a smaller sized heterocarbocyclic ring. Study of the behaviour of PEO-co-VP in the hydrate-forming solution may provide further information on the inhibition mechanism of PEO-co-VP alone and the synergistic effect of PEO-co-VP with TIs.

As shown in Figure 2.9, a full range UV-Vis spectrum scan was conducted using the stock sodium chloride solution consisting of 0.01% PEO-co-VP versus the baseline (stock sodium chloride solution), which shows the maximum wavelength to be 205 nm at room temperature of 24±2 °C. Hence, this wavelength was used to characterise the concentration of the KHI.

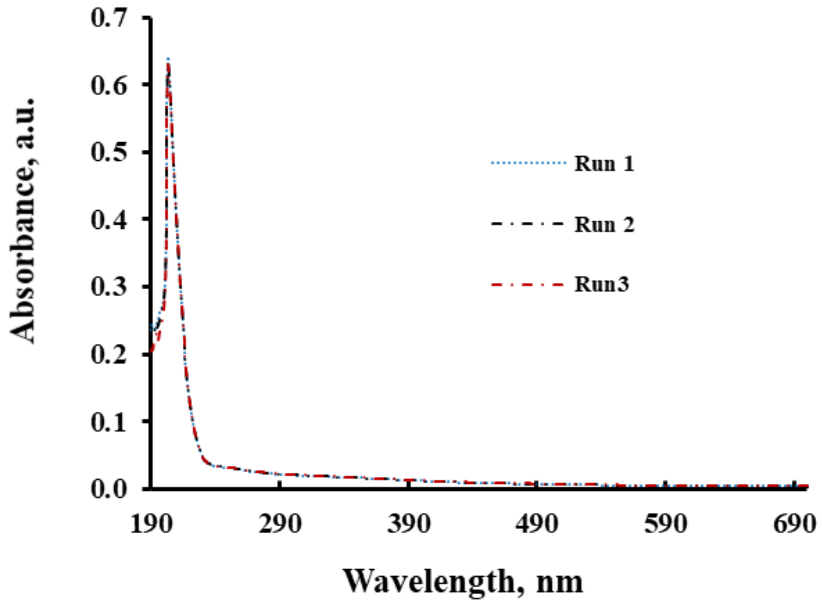

Fig. 2.9 UV-Vis spectrum for 0.01% PEO-co-VP solution

At this wavelength (205nm), a standard curve was established to correlate the absorbance and the concentration of the KHI, as shown in Figure 2.10. Solutions with known KHI mass concentrations of 0.0004%, 0.0008%, 0.002%, 0.003%, 0.004%, 0.006%, 0.009%, 0.012% and 0.012% were prepared using 25 ml volumetric flasks. Each concentration was tested in triplet to obtain an average value for absorbance. The concentrations and their absorbance values demonstrated a clearly linear relationship, through curve fitting. The R-square (R^2) value of the fitting equation was 0.9942. As a result, this curve was used to determine the KHI concentration from samples collected during hydrate formation in the presence of PEO-co-VP.

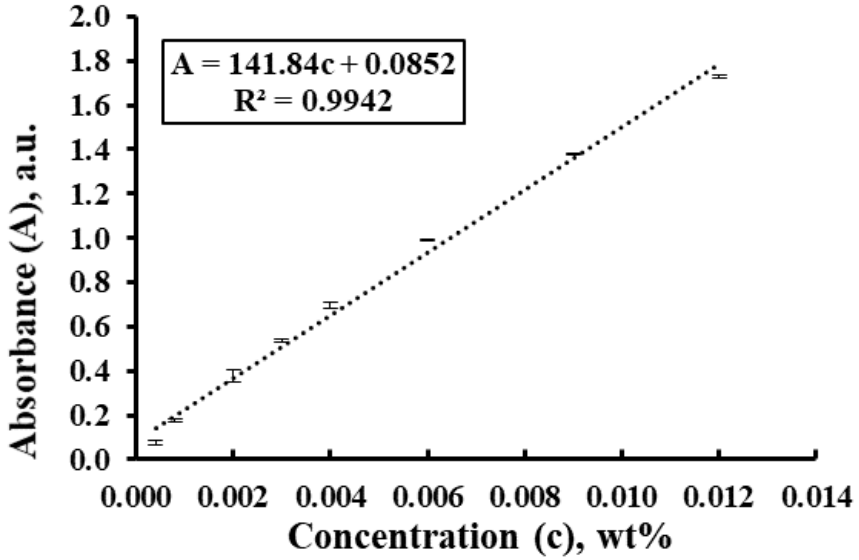

Fig. 2.10 Calibration curve (PEO-co-VP in 3.5% NaCl)

Similarly, a calibration curve was established at 205 nm for the mixed KHI and MEG inhibition system, where PEO-co-VP and 15% MEG in sodium chloride solutions were used for gas hydrate inhibition (Fig. 2.11). A series of standard solutions consisting of 0.0008%, 0.002%, 0.005%, 0.01% and 0.015% KHI in the presence of 15 % MEG were used. The linear absorbance-concentration relationship is clearly demonstrated, with an R^2 value of 0.9962.

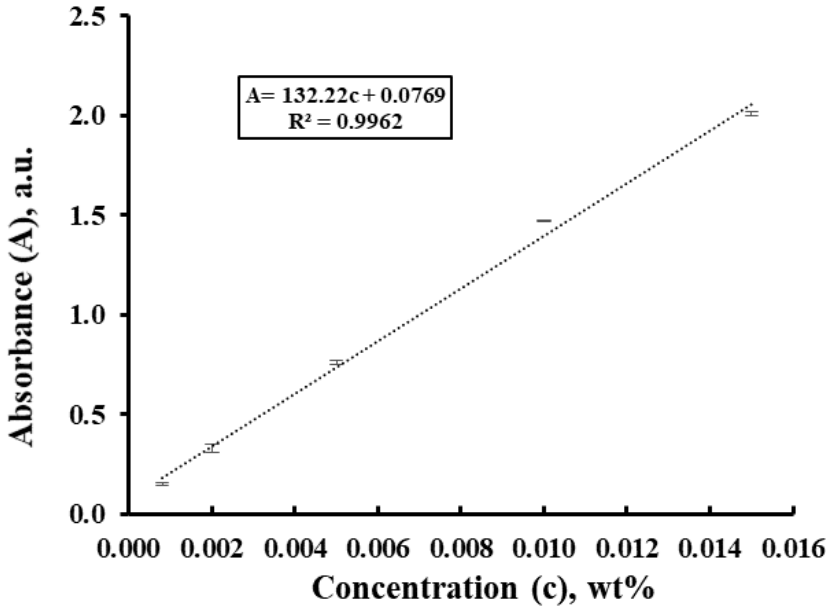

Fig. 2.11 Calibration curve (PEO-co-VP in 15% MEG)

A separate calibration curve was established for the PEO-co-VP and MeOH inhibition system at 205 nm, as shown in Figure 2.12. The calibration curve was established using standard solutions consisting of 0.0008%, 0.002%, 0.005%, 0.01% and 0.015% KHI in the presence of 15% MeOH.

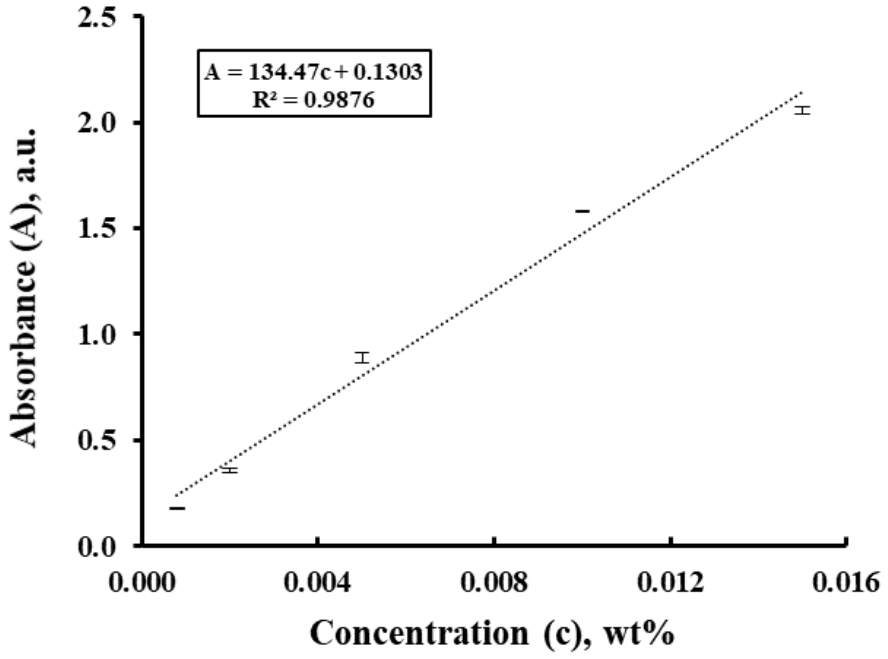

Fig. 2.12 Calibration curve (PEO-co-VP in 15% MeOH)

Chapter 3 Synergistic Effect of MEG with PEO-co-VP

This chapter reports on the experimental investigation into the synergistic effect of MEG with the kinetic inhibitor PEO-co-VP. The influences of temperature, concentration of KHI and concentration of MEG upon the inhibition performance were systematically investigated. Hydrate-forming solutions containing PEO-co-VP and MEG were prepared using the chemical compositions listed in Table 3.1. The solutions were then tested using the experimental set-up and procedures described in Chapter 2. Key parameters, namely, the onset time (t_{onset}), the hydrate growth time (Δt), the percentage of gas consumption (N) and the percentage of hydrate formation (ϕ) were obtained and/or computed to compare the performances of different formulae. Detailed results are presented and discussed in Sections 3.1 to 3.4. Conclusions are presented in Section 3.5.

Table 3.1 Concentrations of KHI and MEG in the testing solutions (3.5% NaCl)

PEO-co-VP, %	**MEG, %**	**T_{set}, °C**
0	0	2, 5.7, 9, 10, 11
0	15	2
0.5	0, 1.5, 3, 5, 10, 15	2
0.75	0, 15	2
1	0	2, 5.2, 8, 9.8
1	1.5, 4.7	2
1	5	2, 5.2, 7, 8
1	10, 15	2

3.1 Inhibition Performance of PEO-co-VP in Absence of MEG

In order to investigate the effect of the concentration change on the KHI performance, hydrate-forming solutions consisting of 0, 0.5, 1 and 1.5% of KHI were tested at a pre-set temperature of 2 ℃, which corresponds to a subcooling value of 12.9 ℃ for 1% KHI and 12.8 ℃ for 0.5% and 1.5% KHI systems. Each solution was tested three times. The blank solution containing 3.5% sodium chloride was also tested for the purpose of comparison. The average values of onset time, growth time and percentage of gas consumed by the end of reactions are presented in Figures 3.1.

As shown in Figure 3.1(a), for the blank solution, the nucleation started immediately after the agitation commenced, therefore t_o = 0 min. After the addition of KHI at concentrations of 0.5%, 1% and 1.5%, the onset times lengthened to 21, 11.8 and 4.3 min, respectively. The increase in onset time was significant, with p values less than 0.05 in all cases. It is interesting to note that, within the tested concentration range, the onset time decreased with the increase of KHI concentrations. The onset time is commonly used to describe the delay of hydrate formation in the presence of inhibitors. It is an indication of the nucleation and likely initial growth that is unable to be detected from the nucleation stage using current technology. The results of this work showed that, in the presence of KHI, the hydrate onset is generally postponed but not to a great degree, which could be due to the chemical insensitivity of the KHI under relatively high subcooling conditions. The reduction in onset time with increasing concentrations of KHI could be a result of the catastrophic growth of hydrates induced by the KHI. Similar observations have been reported by Kumar *et al* (2008) on the inhibition performance of 0.1-1% PVP at subcooling of over 13 ℃. A separate study using the rate of gas consumed further demonstrated that the accelerated growth is likely to be attributable to the high concentration of KHI (Cha et al., 2013b). In the same paper, Cha *et al* speculated that the catastrophic growth of hydrates was due to the formation of the large quantity of $5^{12}6^2$ labile clusters when PVP and PVCap were present (as illustrated in Figure 1.1). These clusters are the essential structures required to form sI hydrate, which possibly initialises the heterogeneous nucleation of sII hydrates.

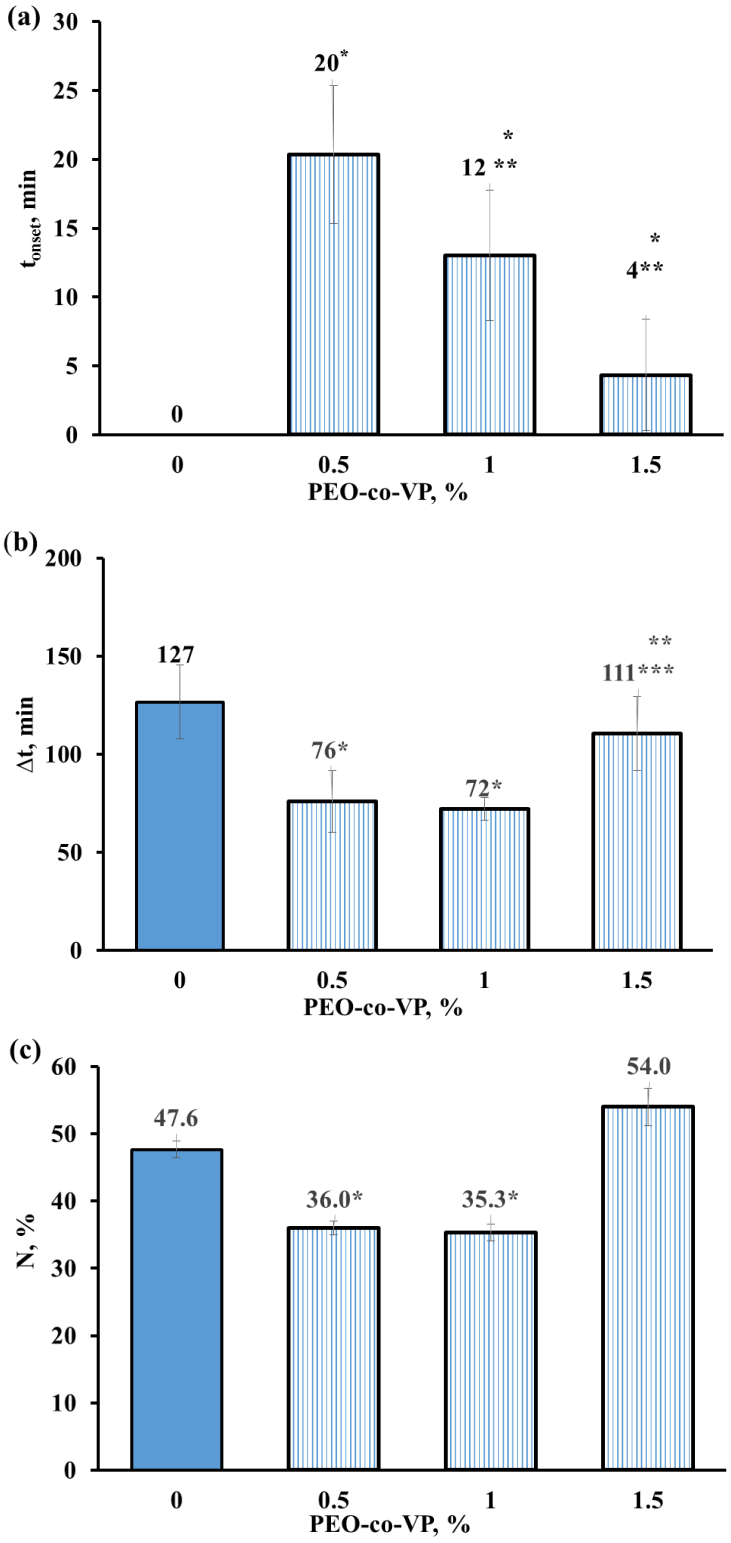

Fig. 3.1 The effect of PEO-co-VP concentration on (a) onset time, (b) growth time and (c) percentage of gas consumption

*, ** and *** denote $p<0.05$ when comparing the result with that of 0%, 0.5%, and 1 % PEO-co-VP, respectively.

For the KHI (PEO-co-VP) used in this study, contains the same pendent group of VP, which might have led to the reduced onset time and/or the accelerated initial growth of gas hydrates.

The presence of KHI in concentrations of 0.5% and 1% reduced both the growth time and the percentage of gas consumption when compared with the results of the blank, as can be seen in Figures 3.1(b) and 3.1(c). In contrast, the differences between the results of the blank and 1.5% KHI solutions were insignificant. As discussed before, this could be a result of the catastrophic growth of hydrates at the high KHI concentrations.

For a more detailed examination, the percentage of hydrate conversion (which is calculated according to Eq. 2.3 in Chapter 2) was plotted against the time (Fig. 3.2). The times required from hydrate onset (t_{onset}) to 80% (t_{80}) hydrate conversion are listed in the insert table. Rapid linear growth was observed for the hydrate-forming solutions containing 0.5% and 1.0% KHI, taking only 24 and 28 min, respectively, to reach 80% hydrate conversion after hydrate onset. In contrast, it took 52 min for the blank solution and 37 min for the 1.5% KHI system to reach the same level of hydrate conversion. Interestingly, the figures showed that increase of the percentage of hydrate conversion went two clear stages in the 1.5% KHI system. This possibly demonstrated that catastrophic growth was promoted by the KHI during the early stage of growth and the following reduced growth was due to the mass transfer limitation at the later stage (Daraboina et al., 2013a). Further investigation is needed to confirm the hypothesis. It should be noted that the slopes are steep during the initial stage (Fig. 3.2) but the rise decreases with increasing KHI concentration, indicating the kinetic effect of the PEO-co-VP.

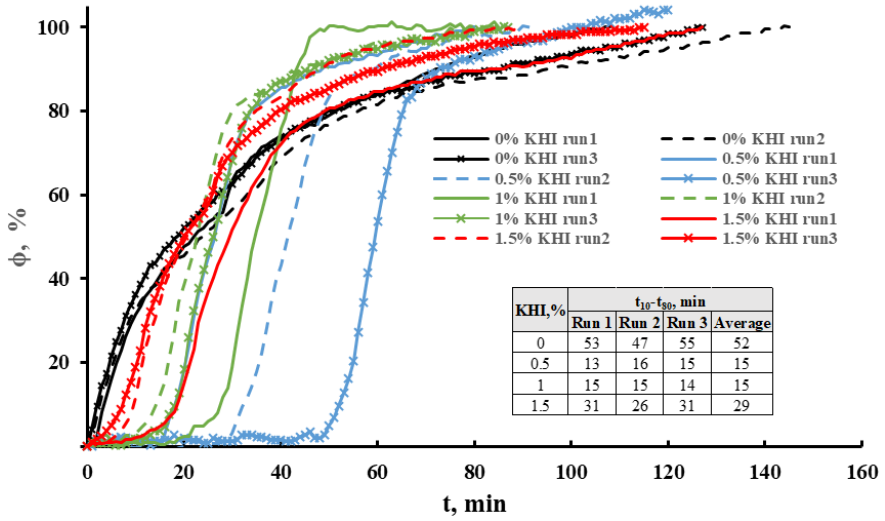

KHI,%	t_{10}-t_{80}, min			
	Run 1	Run 2	Run 3	Average
0	53	47	55	52
0.5	13	16	15	15
1	15	15	14	15
1.5	31	26	31	29

Fig. 3.2 The percentage of hydrate conversion with PEO-co-VP concentrations of 0.5%, 1% and 1.5%

3.2 The Effect of MEG on the Inhibition Performance of KHI

In this section, the effect of MEG and its concentration on the inhibition performance of PEO-co-VP will be reported. The selected KHI concentrations included 0.5% and 1%. The investigated concentrations of MEG ranged from 0 to 15%. The pre-set temperature and the initially charged pressure were 2 °C and 7 MPa, respectively.

3.2.1 Onset time

Figure 3.3 displays the onset time of the hydrate-forming solutions containing 0.5% KHI and MEG of varying concentrations. The result of the solution containing 15% MEG without KHI was added for comparison. There was an increase in the onset time with the increasing concentration of MEG. For example, the onset time was 95 min once 15% MEG was added, compared with 21 min for the solution containing 0.5% KHI only, and 57 min when there was only 15% MEG within the system. A clear synergistic effect has been demonstrated. The increase of MEG concentrations has demonstrated a positive correlation with onset time. This result is consistent with the previously reported work showing that MEG improved the KHI inhibition performance on THF hydrate inhibition (Foo et al., 2016).

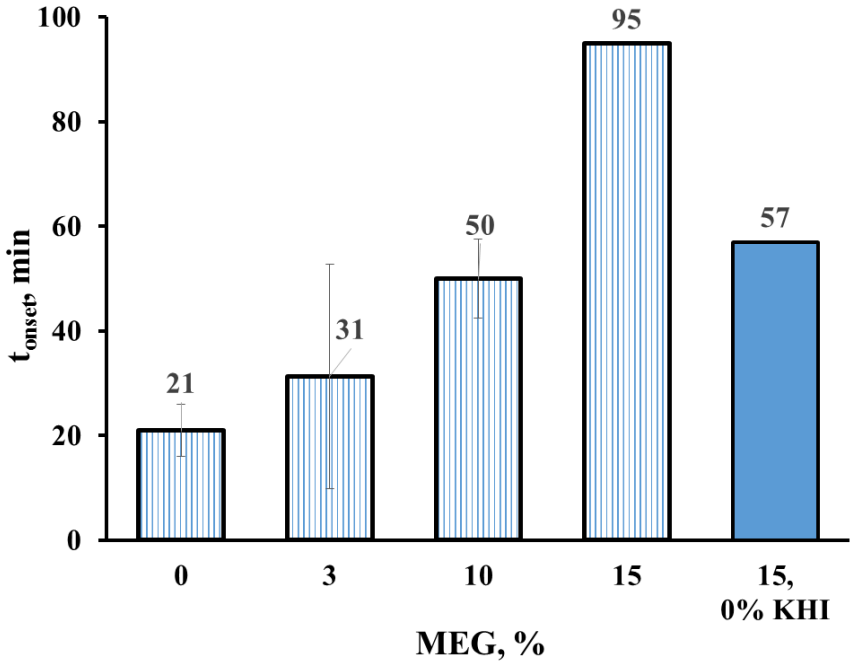

Fig. 3.3 Onset time for 0.5% PEO-co-VP and MEG of varying concentrations

Similar tests were conducted with the solutions containing 1% PEO-co-VP. As shown in Figure 3.4, the trend was similar to the results for solutions containing 0.5% KHI. An apparent increase in the onset time was observed when MEG was added. In addition, a strong synergistic effect was demonstrated in the presence of 15% MEG and 1% KHI. No sign of hydrate onset was observed for the test period of 6,000 min. That inhibition time was much longer than the sum of those for the solutions containing 1% KHI or 15% MEG alone. A positive relationship between the MEG concentration and the onset time is shown in the figure. The distinctive inhibition was observed at a MEG concentration of 10% (15% MEG for 0.5% PEO-co-VP). Below this concentration, the delay in onset of hydrate formation was less obvious.

When comparing the results displayed in Figures 3.3 and 3.4, a similar trend is demonstrated, i.e., at the same MEG concentration, the higher is the KHI concentration, the later is the onset time.

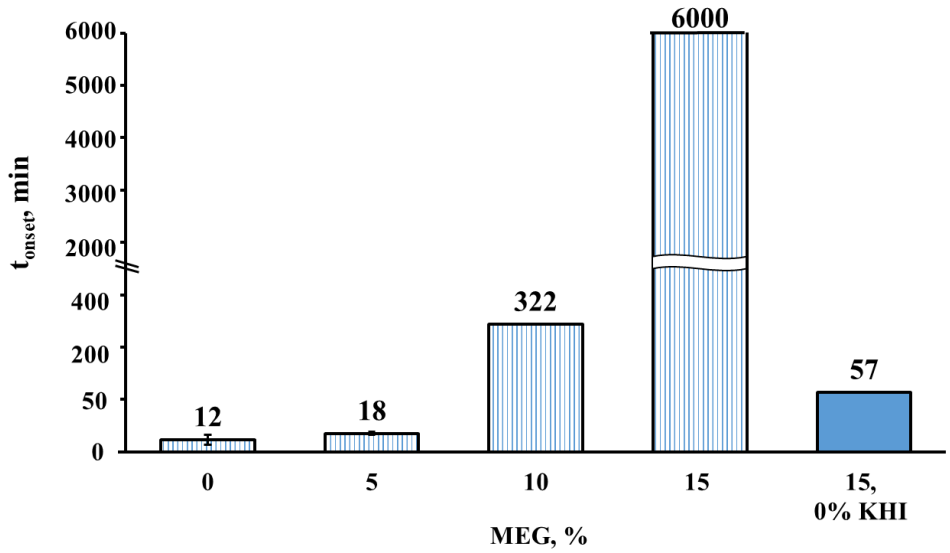

Fig. 3.4 The onset time for 1% PEO-co-VP and MEG of varying concentrations

When looking at the effect of MEG alone, MEG molecules are unlikely to form clathrates with water molecules during the formation process because the concentration of MEG has been reported to increase during the remaining liquid phase (Kim et al., 2014). In fact, Kim *et al* (2014) reported that MEG showed some kinetic effect on hydrate inhibition through its clustering activity with neighbouring water molecules. It has been noted that, at MEG concentrations exceeding 10%, a clustering effect is generated with adjacent water molecules to delay hydrate onset (Kim et al., 2014). This effect is claimed to be due to the hydrogen bonds between the hydroxyl groups of the MEG and the adjacent water molecules. When looking for water molecules alone in the presence of MEG, their activities were noted to improve because the lifetime of hydrogen bonds between water molecules increased by nine times with the addition of MEG (Olsen et al., 2017). Furthermore, the kinetic inhibition effect of MEG was positively related to its concentration. The onset time was reported to increase nearly threefold when MEG concentration rose from 10% to 30%. The greater is the MEG concentration, the stronger is the affinity of MEG with water molecules in the bulk liquid phase. Therefore, the liquid phase relaxation to hydrate structure was retarded and the rearrangement of water molecules to form hydrate was slowed down (Cha et al., 2013a). The kinetic inhibition mechanism of MEG is consistent with the reported inhibition mechanism, which is attributed to the perturbation of water (Sa et al., 2016).

When further examining the detailed effect of MEG concentration, at low concentrations such as 5%, the changes were little and insignificant, as shown in Figure 3.4. However, when MEG concentration was increased to 10% and 15%, a more dramatic increase in onset time was clearly demonstrated.

Kinetic inhibitors primarily work on the hydrophilic hydrate surface through its polar moieties (Maeda, 2015). The polar and hydrophilic moieties of the KHI in this study are the pendant groups of VP and -O-CH_2-CH_2-. It was reported that the inhibition mechanisms of both PVP and PEO are attributable to the perturbation of the water structure or the adsorption of the polymers onto the formation sites (King et al., 2000; Ding et al., 2010; Lou et al., 2012; Daraboina et al., 2013b). The adsorption of these KHIs is believed to be through their hydrophilic pendant groups attaching to the hydrophilic surfaces of hydrates and water cages, which results in their non-polar carbon backbones facing outwards. When the hydrate particles that are adsorbed by KHI come too close to each other, these non-polar groups generate a repellent force to stop the particles binding with each other. Such repellent forces also help to distance the non-polar gas molecules, preventing the growth of hydrate sites (Kim et al., 2014). The results of these two actions are smaller hydrate particle sizes and slower hydrate growth kinetics. However, as hydrate growth is highly dependent on surface area, and the smaller sizes result in greater surface areas, the overall growth may also be affected by the particle sizes. This may explain the aforementioned observations.

When both MEG and KHI were present in the hydrate-forming solution, the synergistic effect on the onset time was demonstrated. This effect became much clearer when MEG concentration was above 10%. It has been reported that, in the presence of KHI, MEG molecules may form clusters with water molecules (Cha et al., 2013a). These water molecules are then anchored due to the hydrophilic moieties of KHI. This may result in reduced formation of hydrate cages and delayed nucleation in a large scale, yielding the synergistic effect that has been seen with the use of PVP and PVCap (Cha et al., 2013a; Kim et al., 2014). In our study, interaction between KHI and MEG molecules may also occur, which leads to a significantly improved inhibition result when MEG is added to the system at concentrations of 10% and 15%. However, little

synergistic effect was shown at the lower concentration levels, indicating a less dominant effect of the cluster formation.

3.2.2 Hydrate growth time

The growth times of hydrate-forming solutions containing 0.5% PEO-co-VP and MEG in various concentrations (0%, 3%, 10% and 15%) were 76±16, 65±24, 74±24, and 92±30 min, respectively. The result for 15% MEG alone was 98 min. The growth time of the hydrate-forming solution containing 15% MEG and 0.5% KHI (92±30 min) was longer than that for 0.5% KHI only (76±16); however, this difference is not statistically significant.

For 1% PEO-co-VP, the concentration change in MEG showed a much stronger impact on the growth time. The growth times of hydrate-forming solutions containing 1% PEO-co-VP and varying MEG concentrations (0%, 5% and 10%) were 72, 157 and 174 min, respectively. The addition of 10% MEG resulted in the growth time increasing from 72 to 174 min. When MEG concentration was increased to 15%, no hydrate formation was observed after 6,000 min. This is a significant improvement.

During such growth, MEG molecules have been reported to remain in the bulk liquid phase and they are unlikely to accumulate on the hydrate surfaces (Kim et al., 2014). In contrast, the KHI molecules have been reported to adsorb onto the hydrophilic hydrate surfaces during this process (Anderson et al., 2011). Bera *et al* (2012) reported that the adsorption of surfactant changed the wettability of the solid surface. The adsorbed KHI possibly changes the hydrate surface polarity through its non-polar carbon backbone facing outwards. This change may stop the further binding of small hydrate particles. On the other hand, KHI molecules possibly reduce the water molecules' activities at the hydrate/water interface. MEG, at a low concentration, is not able to affect the bulk liquid phase significantly and may affect the KHI molecules adjacent with its non-polar moiety ($-CH_2-CH_2-$). It may primarily work on softening the KHI chains in the solution so that the hydrodynamic volume of KHI expands. KHI adsorption is reduced during growth and it is likely to remain in the bulk liquid phase. These molecules then further perturb water molecules with the assistance of MEG molecules. As a result, the hydrate growth is reduced. With further increases in MEG

concentration, the increased interaction between MEG and water molecules comes to dominate hydrate growth control.

To understand the behaviour of KHI during hydrate growth, liquid samples were taken from the solutions containing 0.5% KHI and 0.5% KHI in the presence of 15% MEG. UV-vis was used to test the KHI concentrations of all samples. For both solution concentrations, the first sample was taken at 0 minute prior to the agitation, where no hydrate formed. The following four samples were taken at 48, 68, 98 and 128 min for solutions containing 0.5% KHI and 15% MEG. (The onset time was 41 min.) For the system containing 0.5% KHI only, liquid samples were extracted at 37, 92 and 127 min. (The onset time was 1 min.) This means that samples other than the first were taken during the growth stage of gas hydrates.

As shown in Figure 3.5(a), for the hydrate-forming solutions in the absence of MEG, the KHI concentration in the liquid phase decreased with time. Similar observations were reported by our group when the THF hydrates system was investigated (Foo et al., 2016). The reduced concentration of KHI in the remaining liquid phase was reportedly due to the adsorption of KHI molecules onto the hydrate surfaces during the hydrate growth time. However, an ascending trend was shown with the KHI concentration changes in the test solutions after 15% MEG and 0.5% KHI (Fig. 3.5(b)). This could be a result of the presence of MEG in the system. The strong affinity between the KHI and MEG weakened the interactions between KHI molecules and hydrate surfaces. During growth, the remaining KHI and MEG in the liquid phase continuously interacted with surrounding water molecules. The growth time of 0.5% KHI and 15% MEG was much longer than that of 0.5% KHI alone, indicating that the presence of MEG helped to improve the growth inhibition effect of KHI. When compared with the result of 15% MEG alone, the increase in the growth timeis was less noticeable. This possibly indicates that the growth inhibition was mainly attributable to the MEG.

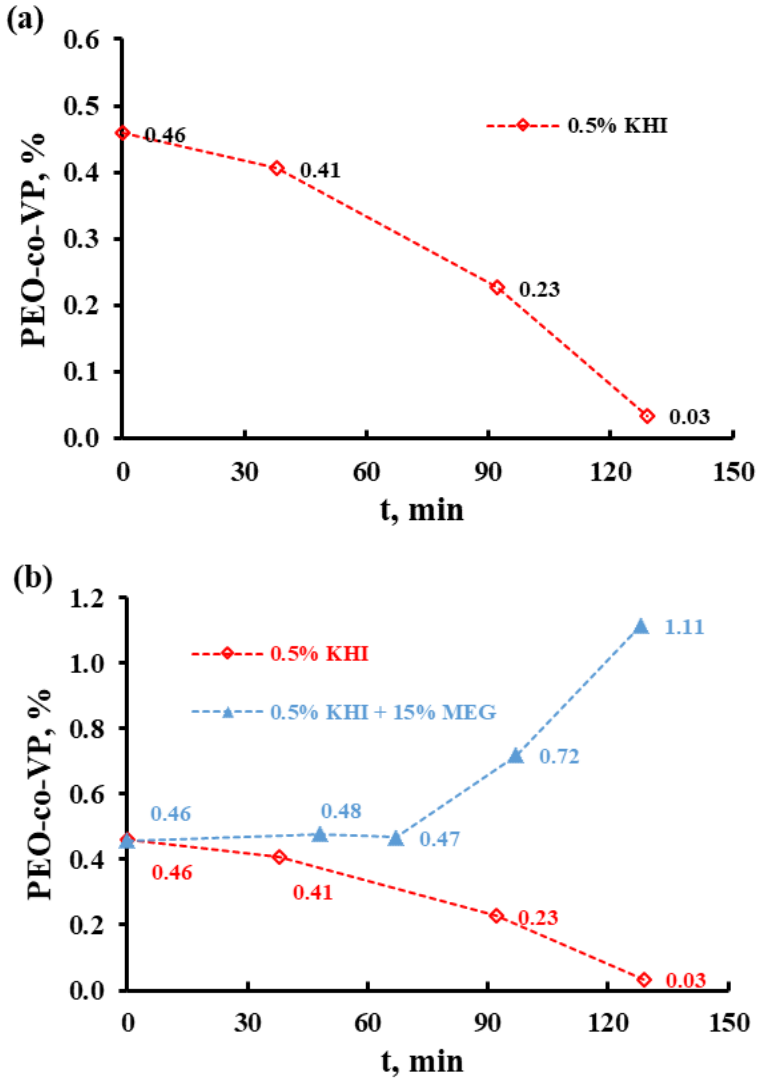

Fig. 3.5 PEO-co-VP concentrations during hydrate growth in (a) 0.5% KHI and (b) 0.5% + 15% MEG solutions

3.2.3 The overall percentage of gas consumption

The overall gas consumption levels of the aforementioned formulae are displayed in Figure 3.6. A negative correlation was observed between MEG concentration and gas consumption in both systems. We know that both MEG and KHI molecules are hydrophilic, meaning that they interact with water molecules via hydrogen bonds. These activities distort continuity of water clusters, therefore reducing the number of water clusters formed and leading to reduced gas consumption. At high MEG concentrations, the distortion could be dominated more by the presence of MEG, as demonstrated by the gas consumption (18.5%) when no KHI was present. When KHI was also used in the hydrate-forming solutions, the overall percentage of gas

consumption was further reduced, indicating that effect of KHI on gas consumption is not predominant.

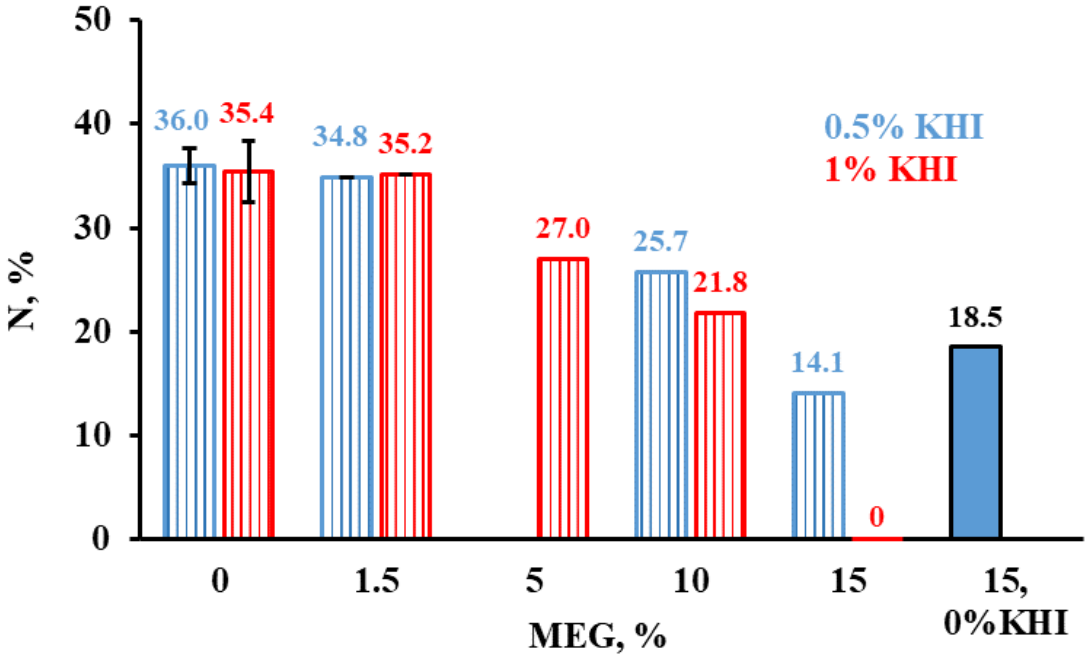

Fig. 3.6 Percentage of gas consumption (N) of 0.5% KHI and 1% KHI with varying MEG concentrations

3.3 The Effect of KHI Concentration on the Overall Performance of Synergists

The contribution of KHI concentration towards the overall synergistic effect was investigated with a fixed MEG concentration of 15%. The onset times and growth times are shown in Figure 3.7. The results of the solution containing 15% MEG was included for comparison.

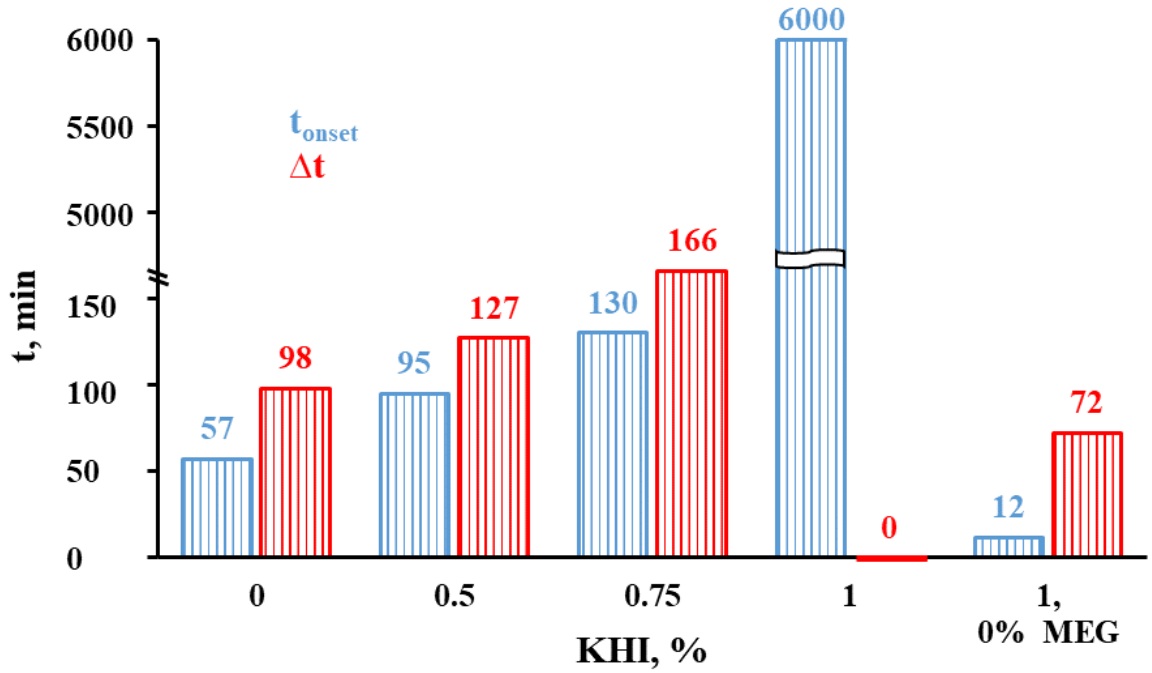

Fig. 3.7 Onset time (t_{onset}) and growth time (Δt) of hydrate-forming solutions containing 15% MEG and varying concentrations of PEO-co-VP

Both the onset time and the growth time increased with increasing concentrations of KHI. For the system containing 1% KHI and 15% MEG, no formation of hydrates was observed. The experiment was terminated after 6,000 min operation.

The previous results in Section 3.1 indicated that, with PEO-co-VP alone, increasing the concentration may introduce heterogeneous nucleation that causes a catastrophic growth of hydrates. With the presence of MEG, no catastrophic growth was observed. This further demonstrates the synergistic effect on nucleation inhibition between PEO-co-VP and MEG.

As shown in Figure 3.8, the percentage of gas consumption demonstrated a downward trend as KHI concentration increased. No gas hydrate formed when the KHI concentration was increased to 1%. The effect of MEG (15%) on the reduction of gas consumption was much more significant than that of KHI (1%). This is possibly attributable to the MEG molecules that remained in the liquid phase, which stopped the free water forming complete cage structures.

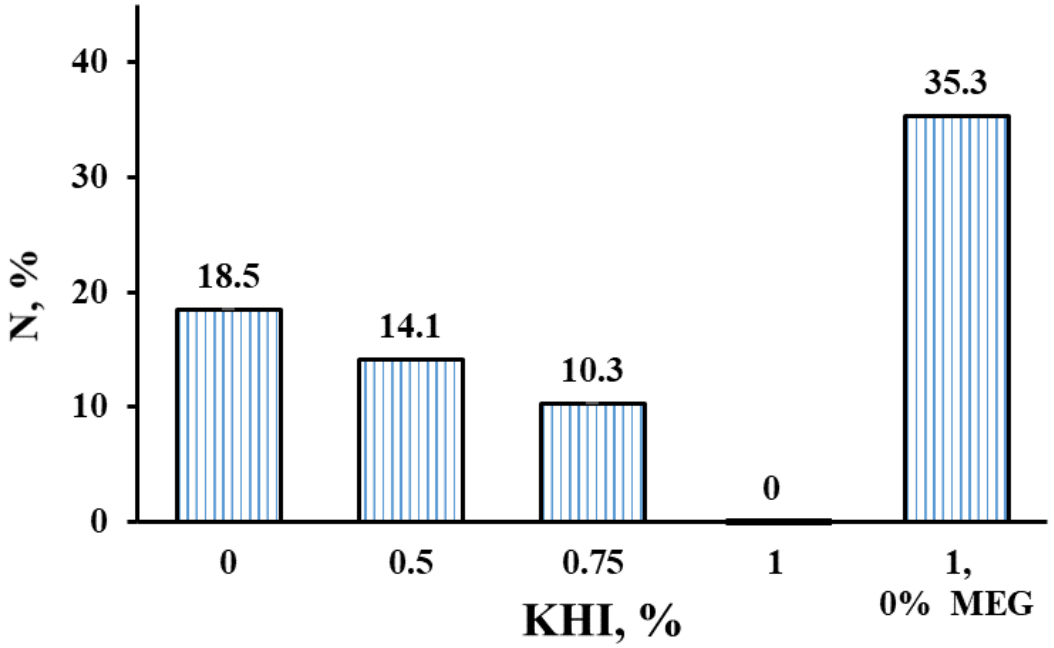

Fig. 3.8 Gas consumption (N) of 15% MEG and PEO-co-VP in varying concentrations

3.4 Temperature Effect on Inhibition Performance

3.4.1 PEO-co-VP without MEG

In this section, the temperature effect on the inhibitor performance of 1% PEO-co-VP is reported from testing at 2.0°C, 5.2 °C, 8.0 °C and 9.8 °C. The onset time (t_{onset}), the growth time (Δt) and the percentage of gas consumption (N) at the completion of reactions are listed in Table 3.2. The calculated equilibrium temperatures (T_e) by CSMGem at the experiment pressure (P_{exp}) and the corresponding subcooling temperature (T_{sc}) at each pre-set temperature are also summarised in the same table.

Table 3.2 Hydrate formation with 1% PEO-co-VP at 2.0, 5.2, 8.0 and 9.8 °C

T_{set}, °C	P_{exp}, MPa	T_e, °C	T_{sc}, °C	t_{onset}, min	Δt, min	N, %
2.0*	6.4	14.9	12.9	12±5	72±6	35.3±2.8
5.2*	6.5	15.0	9.8	17±1	83±4	37.1±0.6
8.0	6.6	15.1	7.1	119	383	11.8
9.8	6.7	15.2	5.4	2,187	183	16.1

*Hydrate formation tests were conducted in triplicate and the results were averaged.

With increasing temperature, an ascending trend was observed in the onset time, which is largely due to the decrease in the driving force (subcooling). It is well accepted that subcooling is the main driving force for hydrate formation. At 2.0 °C, the corresponding subcooling temperature was around 12.9 °C and the observed average onset time was 12 min. Increasing the set temperature from 2.0 to 5.2 °C correlated with a reduction in subcooling from 12.9 to 9.8 °C, and resulted in a slight increase in onset time of 5 min. A further reduction of subcooling to 7.1 and 5.4 °C led to a further delay in the onset times to 119 and 2,187 min, respectively. The onset time was plotted against the reciprocal of T_{sc} (°C), as shown in Figure 3.10, which fits well with the Arrhenius equation (Equation (1), R^2 is 0.96), thus

$$t_{onset} = \boldsymbol{a} \times e^{\frac{\boldsymbol{b}}{T_{sc}}} \qquad (1)$$

where ***a*** is 0.16 and ***b*** is 49.85. This equation is commonly used to describe the kinetic growth of gas hydrates (Englezos et al., 1987). According to Englezos, the driving force is the combined effect of pressure, temperature, water-gas interfacial area and degree of supercooling, which could be reflected in the values of ***a*** and ***b*** in Equation (1). In this particular experiment, the effect of the degree of subcooling on the inhibition performance of the KHI-MEG combination can be shown by the values of ***a*** and ***b.*** More discussion of this can be found in Section 4.3.

The largest increase in the onset time was observed when the temperature was raised from 8.0 to 9.8 °C, which corresponded to a change of 1.7 °C in subcooling. A similar test of the blank solution was conducted at five different temperatures, namely 2.0, 5.7, 9.0, 10.0 and 11.0 °C. The corresponding onset times were 0, 4, 43, 60 and 2,102 min, respectively. The plots between onset time and subcooling temperature for the blank and KHI + 5% MEG were added to compare with the result for 1% KHI (Fig. 3.9). All collected data for the blank are shown in Table 3.3.

Table 3.3 Hydrate formation with the blank at 2.0, 5.7, 9.0, 10.0 and 11.0 °C

T_{set}, °C	P_{exp}, MPa	T_e, °C	T_{sc}, °C	t_{onset}, min	Δt, min	N, %
2.0*	6.4	14.8	12.8	0	127	47.6
5.7	6.5	15.0	9.3	4	134	34.4
9.0	6.7	15.1	6.1	43	152	22.7
10.0	6.7	15.2	5.2	60	201	18.8
11.0	6.7	15.2	4.2	2102	200	19.5

*Hydrate formation tests were conducted in triplicate and results were averaged.

As for the 1% KHI system, an upwards trend for onset time was demonstrated at the elevated pre-set temperatures in the blank solution, as shown in Figure 3.10. The corresponding plotted curve fits with the Arrhenius equation (1) (R^2 is 0.93), where ***a*** is equal to 0.02 and ***b*** is equal to 45.80. The onset time dropped exponentially with the increase in subcooling for both the blank and the 1% KHI system. The constant ***b*** is much greater for 1% KHI than for the blank, indicating a rapid approach and accelerated effect on the relationship between the onset time and subcooling. This is similar to the findings of Anderson *et al* (2011) in the formation of methane hydrate in the presence of PVCap.

It is well known that the inhibition performance of KHIs is sensitive to the degree of subcooling. In general, KHIs show reliable inhibition performance under lower subcooling conditions. However, their applications are normally limited to 10.0 °C (Kelland, 2006).

It is interesting to see that the growth time also increased at the elevated set-temperature (Table 3.2). The growth time peaked at 383 min at 8.0 °C. Although a shortened growth time was observed when the pre-set temperature was further increased to 9.8 °C, the total reaction time made up by the onset time and the growth time were still largely reduced.

The percentage of gas consumption was much higher at the lower temperatures (2.0 and 5.2 °C) than for higher temperatures (8.0 and 9.8 °C). This is not unexpected because hydrate formation is more favourable at lower temperatures (Veluswamy et al., 2018). However, when the pre-set temperature was 8.0 °C, the overall percentage of consumption was reduced to the lowest level of 11.8%. The gas consumption at 9.8 °C (16.1%) was higher than that at 8.0 °C, which is possibly attributable to a much longer formation period. The reduced gas consumption is a result of increased activity between the KHI and water molecules at the elevated temperature in the presence of KHI (Foo et al., 2016).

3.4.2 PEO-co-VP with 5% MEG

A similar study was carried out when 5% MEG was added into 1% KHI. In this case, the investigated pre-set temperatures were 2.0, 5.2, 7.0 and 8.0 °C. The results are shown in Table 3.4. It can be seen that there is an apparent increase in the onset time at elevated pre-set temperatures. This shows a similar trend to that observed in the previous section.

Table 3.4 Hydrate formation with 1% PEO-co-VP and 5% MEG at 2.0, 5.2, 7.0 and 8.0 °C

T_{set}, °C	P_{exp}, MPa	T_e, °C	T_{sc}, °C	t_{onset}, min	Δt, min	N, %
2.0	6.4	14.9 (13.6)	12.9 (11.6)	4	42	30.9
5.2	6.5	15.0 (13.7)	9.8 (8.5)	63	159	23.0
7.0	6.6	15.1 (13.9)	8.1 (6.9)	140	154	22.3
8.0	6.5	15.1 (13.8)	7.1 (5.8)	942	298	12.3

The corresponding data considering TI are included in the parentheses.

The correlation of t_{onset} and T_{sc} also can be described by the Arrhenius equation as shown in Equation (1) in this chapter ($R^2 = 0.97$) with the value of ***a*** being 0.10 and ***b*** being 79.91, and it is shown in Figure 3.9. As can be seen from the equation, the temperature change (the reciprocal of subcooling temperature) shows an even stronger

impact on the onset time when there is 5% MEG in the system. This is not a surprise since the presence of MEG helps the inhibitor to work in the higher subcooling region.

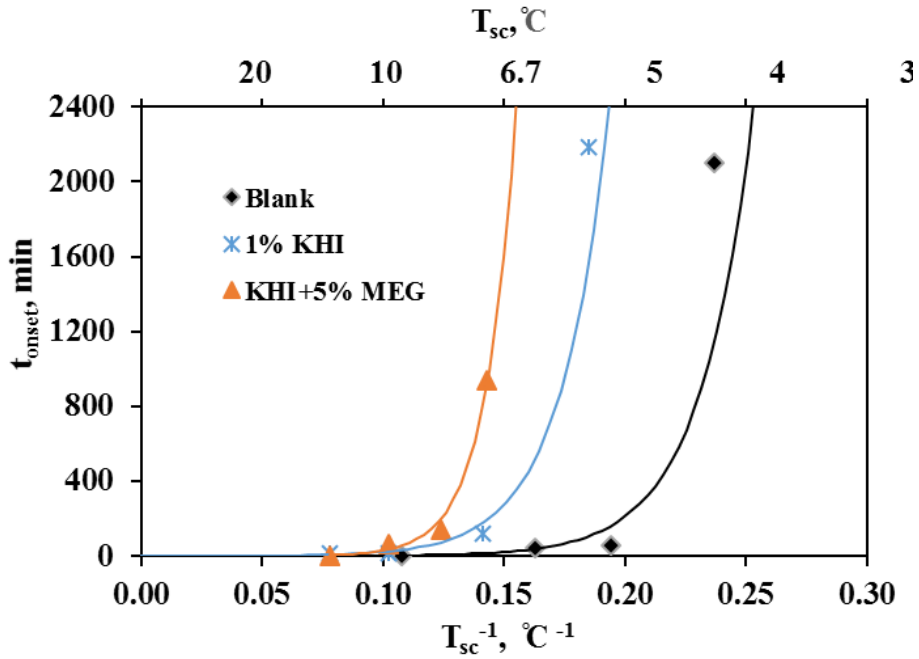

Fig. 3.9 Onset time vs subcooling temperature of 1% KHI + 5% MEG, 1% KHI and the blank

In general, the effect of temperature on inhibition performance of the mixed KHI and MEG was similar to that of KHI alone. The results are presented in Figure 3.10. However, the onset time and growth time both increased when 5% MEG was added into the KHI. In contrast, the overall percentage of gas consumption reduced.

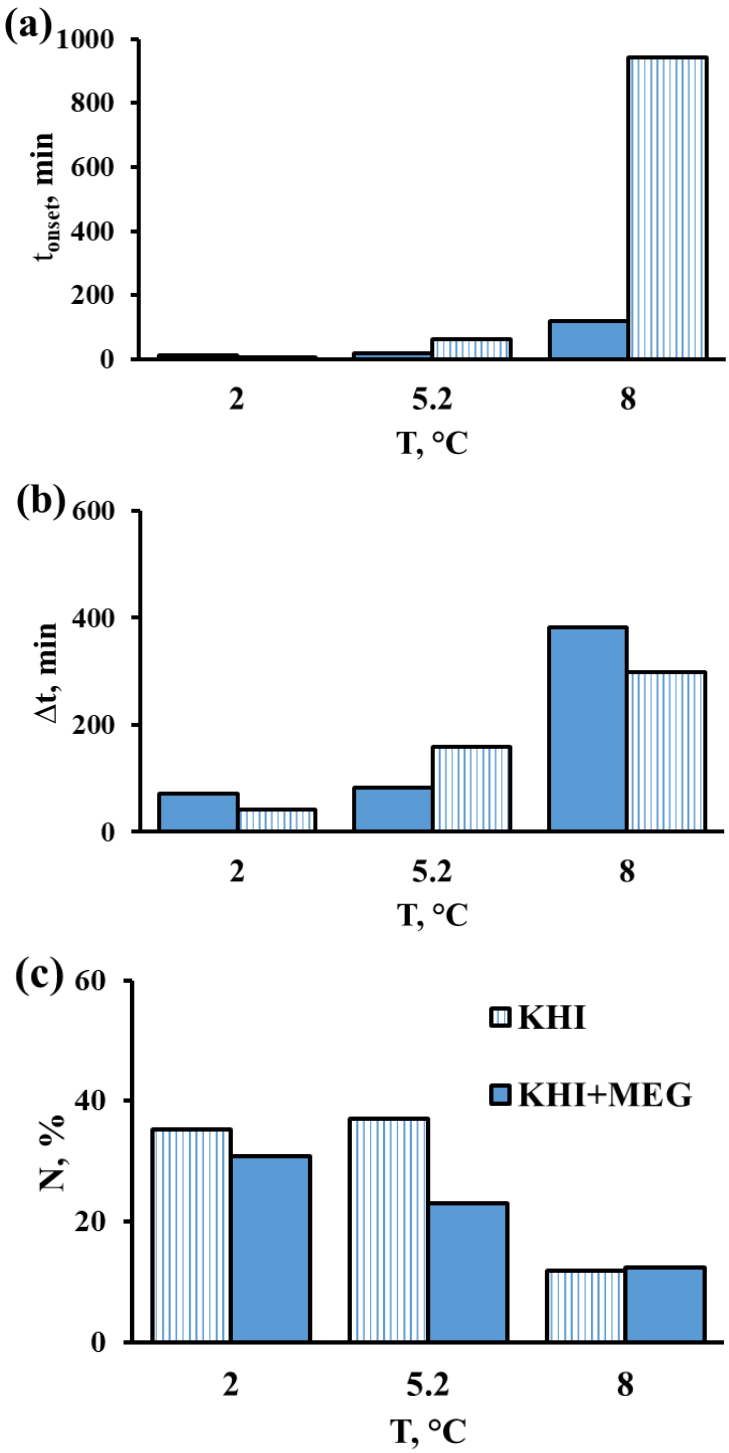

Fig. 3.10 (a) Onset time (t_{onset}), (b) growth time (Δt) and (c) percentage of gas consumption (N) of 1% KHI and 1% KHI + 5% MEG at 2.0, 5.2 and 8.0 °C

3.5 Conclusions

In this chapter, the performance of PEO-co-VP was firstly investigated at subcooling temperatures of 12.9 °C (1% KHI) and 12.8 °C (0.5% and 1.5% KHI). Clear inhibition

was demonstrated using 0.5% and 1% KHI. The inhibition performance was not sensitive to the concentration change due to the high subcooling temperature. Increasing concentration to 1.5% showed no improved inhibition to the formation of gas hydrates. However, the overall hydrate growth time was prolonged with the increased KHI concentration. The reduced inhibition at high concentration of KHI was hypothetically due to the catastrophic hydrate growth induced by the KHI, which also has been reported by other researchers (Kumar et al., 2008; Cha et al., 2013b; Sharifi and Englezos, 2015).

The MEG was then added to the hydrate-forming solution to examine whether there was any synergistic effect to the KHI. A significant increase in inhibition performance was observed in the solution that contained 1% KHI and 15% MEG with no sign of hydrate formation during the test period of over 6,000 minutes, thus demonstrating a clear synergistic effect. The improved performance was also found to correlate with MEG concentration. The increased growth time and the reduced gas consumption were also found to be associated with the increasing concentration of MEG. This possibly resulted from the combined effects of MEG and KHI on the interactions with water molecules during hydrate formation.

To summarise, systematic experiments were conducted to study the effect of a temperature change on the inhibition performance of different hydrate-forming solutions (a blank, 1% PEO-co-VP and 1% PEO-co-VP + 5% MEG). The change of temperature produced similar effects in all tested solutions, which can be described by the Arrhenius equation. The addition of PEO-co-VP moved the curve to a higher subcooling region when compared with the blank. The further shift to the even higher subcooling region was observed when the MEG was added. At the higher subcooling temperatures, the reduction in the onset time of KHI + MEG was much more rapid than that of KHI alone, indicating a more sensitive response of the combined KHI and MEG to the subcooling.

Chapter 4 Synergistic Effect of MeOH with PEO-co-VP

In this chapter, the inhibition performance of PEO-co-VP in the presence of MeOH will be reported. The dosage of the hydrate-forming solutions is detailed in Table 4.1. Sections 4.1 and 4.2 examine the contributions of KHI and MeOH to the total synergistic effect, respectively. Liquid samples were extracted to test the KHI concentrations during the process of hydrate formation. The results were then correlated to determine the possible underlying mechanism. The onset times for the different temperatures at which hydrates formed in the solutions containing 1% KHI and 5% MeOH were tested and compared with the results of the previous section. Conclusions, based on the observations, will be presented in Section 4.4.

Table 4.1 Concentrations of KHI and MeOH in the test solutions (3.5% NaCl)

PEO-co-VP, %	MeOH, %	T_{set}, °C
0	0, 10, 15	2.0
0.5	0, 0.75, 10, 15	2.0
0.75	10	2.0
1	0, 10	2.0
1	5	2.0, 3.0, 4.0, 5.2

4.1 The Effect of MeOH on the Inhibition Performance of PEO-co-VP

4.1.1 Onset time

The onset times for solutions containing 1% PEO-co-VP and MeOH in concentrations of 0%, 5% and 10% are shown in Figure 4.1. The result of the solution containing 10% MeOH but 0% KHI was included in the same figure for comparison. The subcooling

temperatures of the abovementioned solutions were 12.8, 10.8, 8.0 and 8.1 °C, respectively.

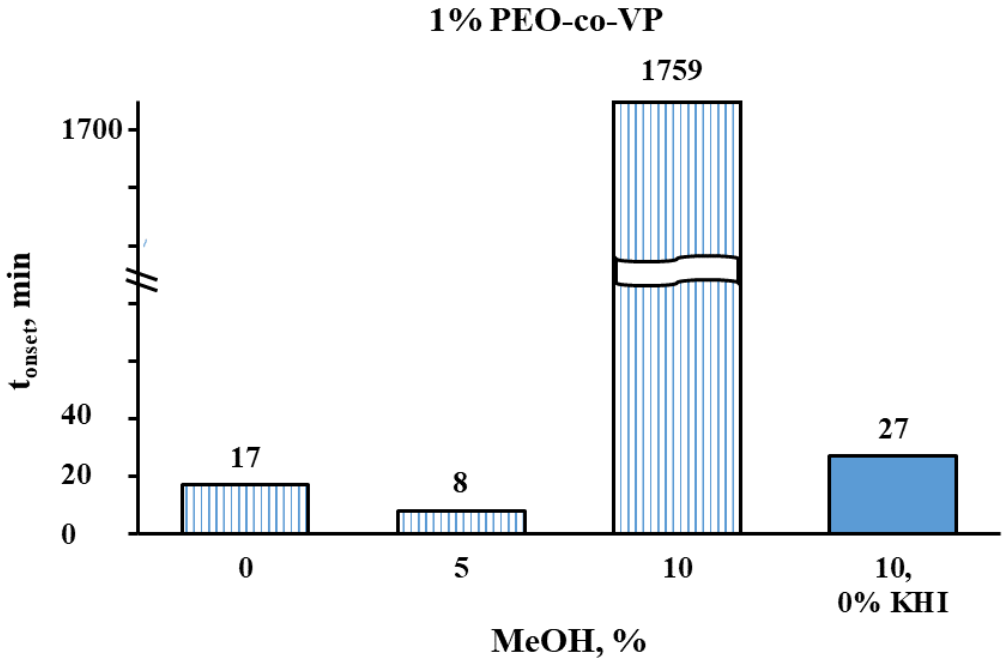

Fig. 4.1 The onset times (t_{onset}) for 1% PEO-co-VP with MeOH in varying concentrations

Without methanol, the onset time was 17 min in the presence of 1% PEO-co-VP. The addition of 5% MeOH resulted in a similar onset time of 8 min. A further increase of MeOH concentration to 10% significantly improved the inhibition of hydrate nucleation, with an onset time of 1,759 min. The onset time was 27 min in the presence of 10% methanol only. A clear synergistic effect was demonstrated by adding 10% methanol to 1% PEO-co-VP.

As shown in Figure 4.2, similar tests were conducted when only 0.5% PEO-co-VP was used. No significant change was observed when the added MeOH concentration was at 0.75, 5 or 10%. Extended onset time was shown only after 15% MeOH was added. This is different from the result for 1% PEO-co-VP, to which only 10% MeOH was sufficient to show the synergistic effect.

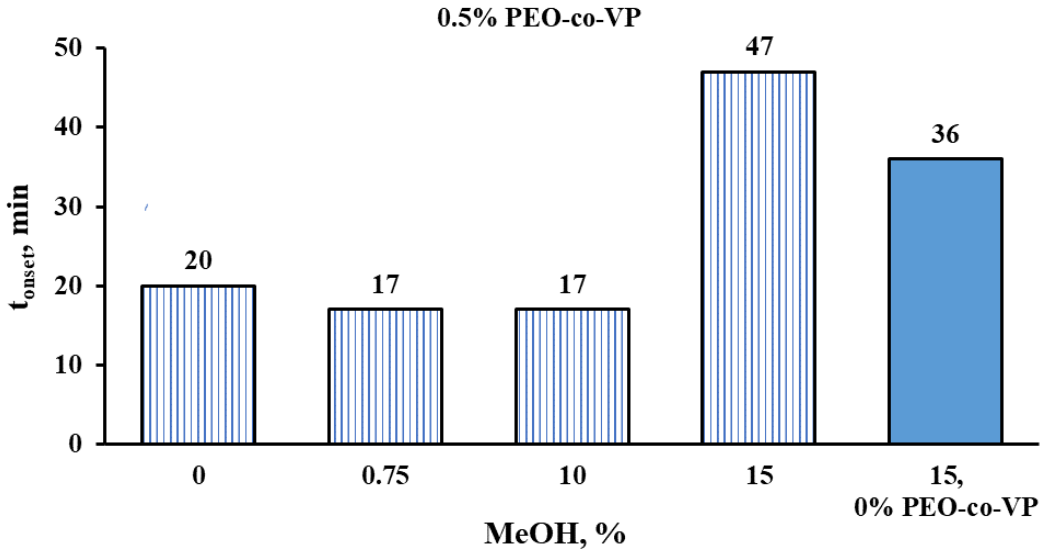

Fig. 4.2 The onset times (t_{onset}) for 0.5% PEO-co-VP and MeOH in varying concentrations

For a given system with a specific inhibitor dosage, the driving force of hydrate formation is inversely proportional to the inhibitor's performance (Cha et al., 2013a). In our investigated system, subcooling is considered to be the main driving force (Sharifi et al., 2014). It is well known that the addition of MeOH can reduce the subcooling temperature, therefore lowering the driving force for the formation of hydrates. This results in increased opportunities for the KHI molecules to interact with the water molecules in the liquid phase, and to form the increased number of hydrogen bonds with water molecules, therefore reducing the onset time. According to the findings of Ke *et al* (2016), MeOH has little effect on nucleation inhibition when compared with KHIs such as PVP and PVCap. This further demonstrates that the increased onset time for the solution (1% KHI + 10% MeOH) is a result of the synergistic effect of MeOH and KHI in the system.

4.1.2 Hydrate growth and gas consumption

The growth times and the percentages of gas consumption of the aforementioned solutions are displayed in Figure 4.3. The result of a solution containing 10% MeOH is included for comparison. As shown in Figure 4.3(a), there is no significant increase in the growth time. The range in growth times of the tested solutions was from 72 to 89 min, except for the solution of 5% MeOH + 1% PEO-co-VP, which showed a much greater value of 125 min growth time. This coincides with the highest gas consumption

rate of 38.0%, as shown in Figure 4.3(b). The results indicate that a longer growth time could lead to higher consumption of the gases. The addition of MeOH showed a negative impact on gas consumption. When PEO-co-VP concentration was 1%, the addition of 10% MeOH reduced the total gas consumption to 12.3%, compared with 35.3% for the solution containing no MeOH. The mixed PEO-co-VP and MeOH outperformed either component individually, resulting in a significantly lower value for gas consumption. This further demonstrates the synergistic effect of the PEO-co-VP and methanol.

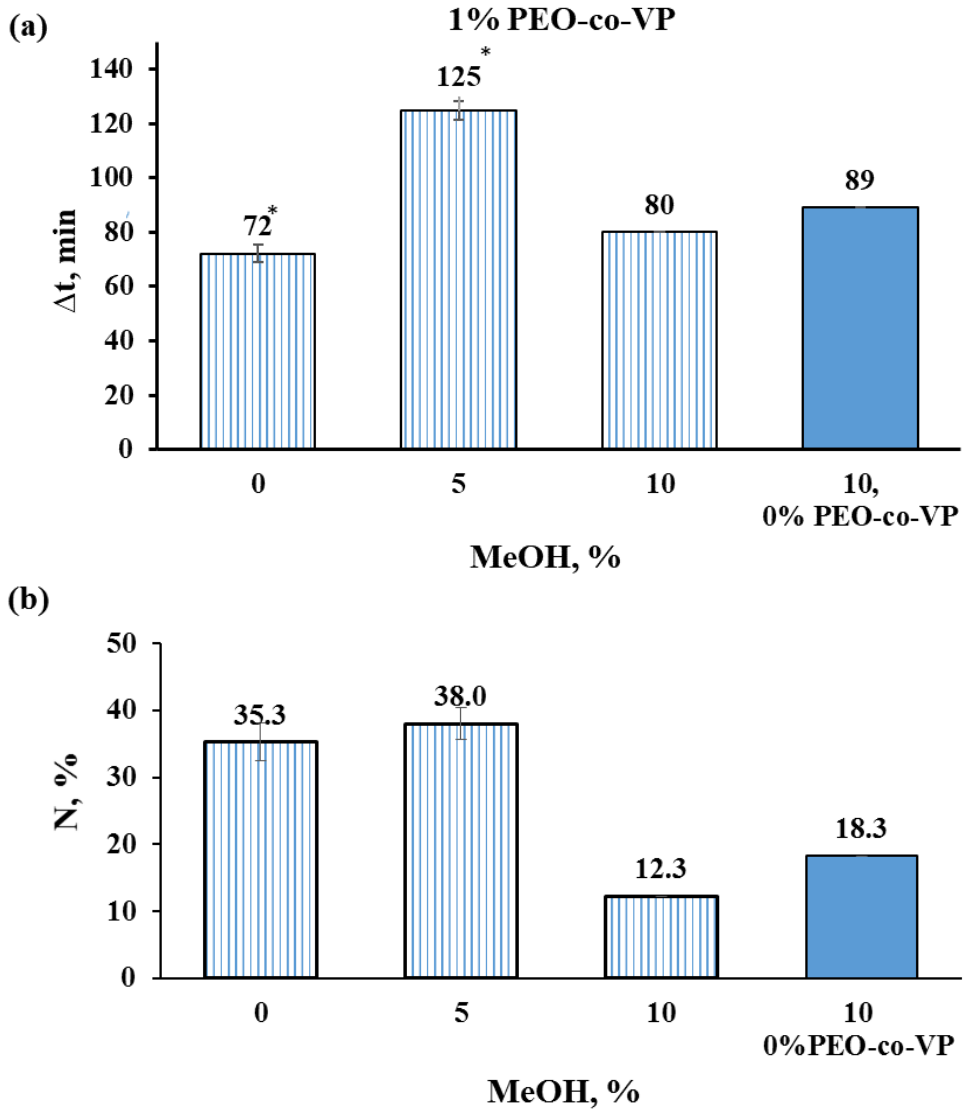

Fig. 4.3 (a) The growth time (Δt) and (b) the percentage of consumption (N) for 1% PEO-co-VP and varying MeOH concentrations

*Average of tests conducted in triplicate, and results were significantly different

Figure 4.4 shows the growth times and the percentages of gas consumption of the hydrates for the system that contained 0.5% KHI. Similar trends were observed as for the series of tests on solutions that contained 1% KHI for both the growth times and the percentages of gas consumed.

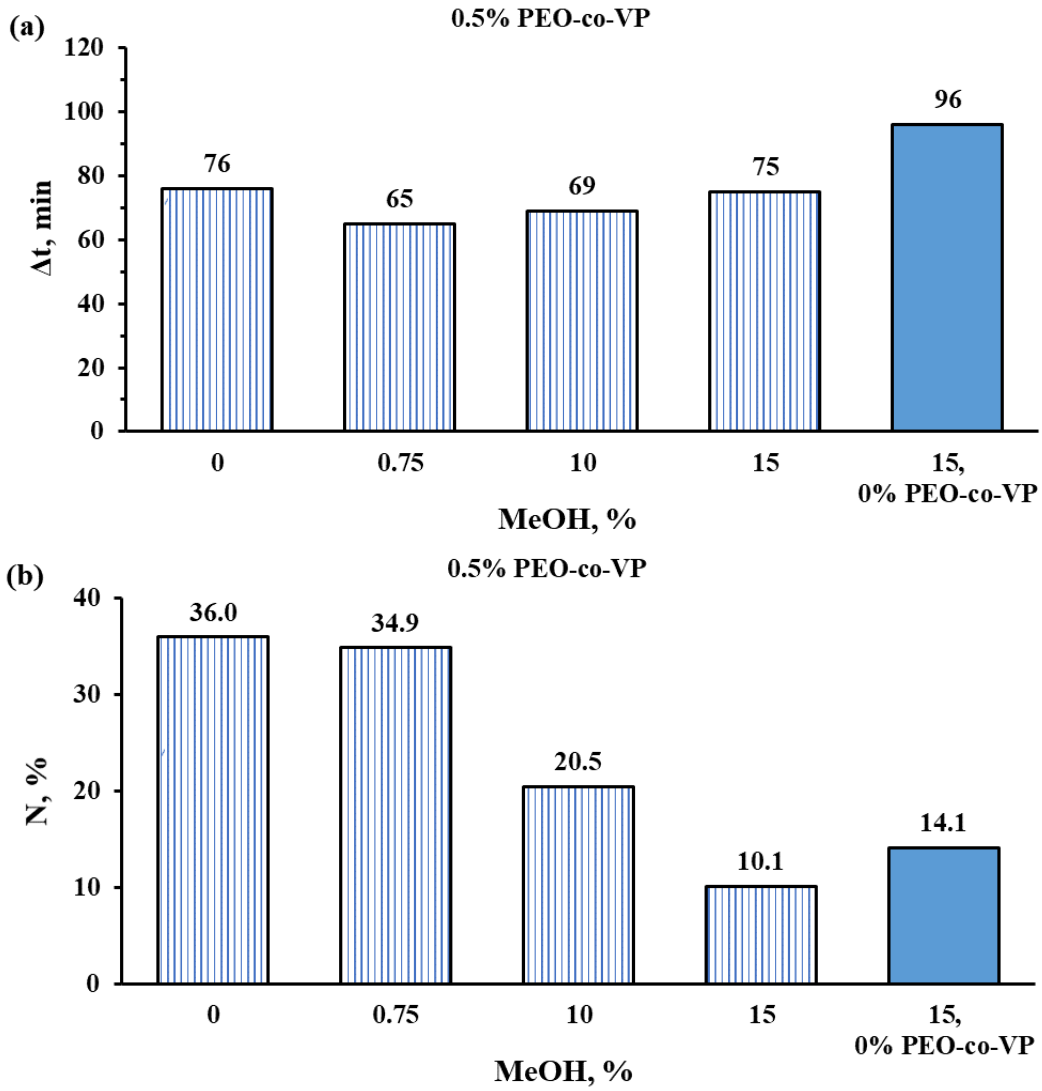

Fig. 4.4 (a) The growth time (Δt) and (b) the percentage of consumption (N) for 0.5% PEO-co-VP and varying MeOH concentrations

To further understand the details of growth, the percentages of hydrate conversion are plotted in Figure 4.5. Data from the period between hydrate onset and 40% conversion were extracted to analyse the initial growth. Linear curve fitting within this period yielded R^2 values greater than 0.97 for all tested systems, indicating that the growth is mainly controlled by mass transfer (Cha et al., 2013a). Compared with the results of

the hydrate-forming solution containing 1% KHI only, the periods of the growth($t_{onset-40}$) in the presence of MeOH were much longer. There is a clear indication of growth inhibition due to the addition of MeOH.

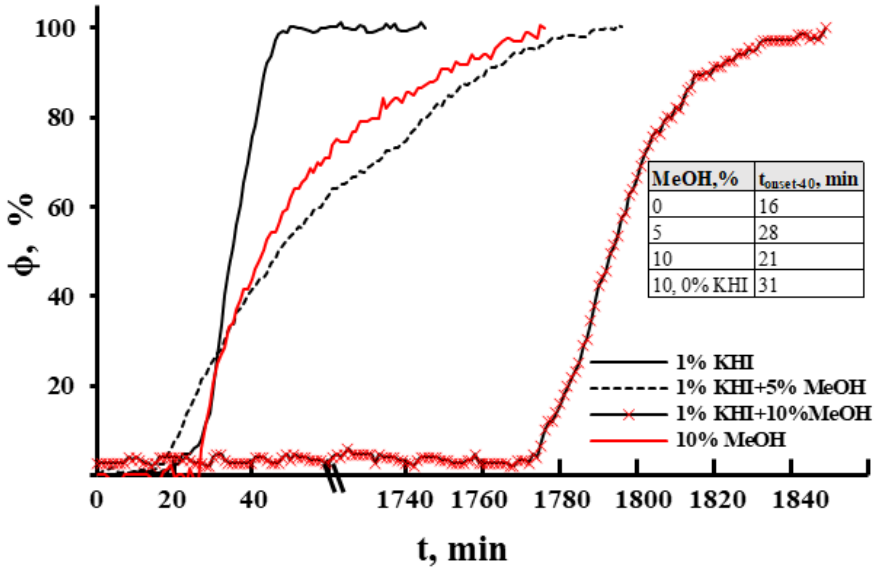

Fig. 4.5 Hydrate conversion (ϕ) for 1% PEO-co-VP and MeOH in varying concentrations

For each reaction, the initial gas was in excess. Hydrate formation was deemed to be terminated when all free water molecules were fully converted to the gas hydrate. When incomplete cages were formed due to the presence of a substance other than gas molecules (methane, ethane and/or propane), less gas was consumed, i.e. the percentage of gas consumption was reduced. The presence of both KHI and MeOH could cause the incomplete cage structure to form, so that gas consumption was reduced. For KHI, Daraboina *et al* (2011) suggested that the chemical groups of KHI may adsorb onto the open cages of the hydrate surface, leading to reduced cage occupancy by gas molecules. On the other hand, MeOH molecules have been reported to directly participate in the formation of a hydrate, with an oxygen atom becoming part of a water cage, during the formation of THF hydrates (Shin et al., 2013). In fact, MeOH tends to join water clusters through its substitution of water molecules when dissolved in water (Wakisaka et al., 1998). This cluster structure is similar to that of a clathrate hydrate and makes it ready to transform into the stable methanol hydrate once a solid phase is formed (Nakayama et al., 1997; Shin et al., 2013). During this process,

the OH^- ions participate as part of the cage and the non-polar moiety CH_3 rotates inside the cavity to act as the guest molecule, as shown in Figure 4.6. Therefore, the total gas consumption is reduced when MeOH and KHI are present in the system and any further reduction is possibly attributable to the increased concentration of MeOH.

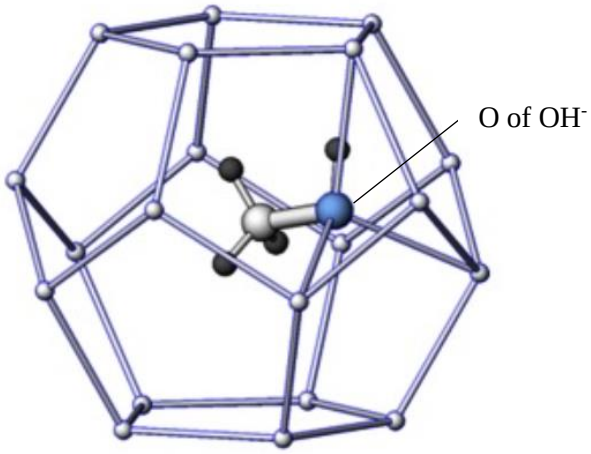

Fig. 4.6 Methanol molecule is incorporated into the water cage (obtained with permission from Shin et al., 2013)

During hydrate formation, the change of PEO-co-VP concentration in the liquid phase was monitored and the results are shown in Figure 4.7. For the hydrate-forming solution consisting of 0.5% KHI and 15% MeOH, the corresponding onset time was 110 min. The first sample was taken at 0 minutes prior to agitation where no hydrate formation had occurred. Following that, samples were taken at 112, 125, 142 and 169 min. The concentration of KHI remained the same until the onset time then increased with increasing time after the initial nucleation, indicating that the KHI molecules remained in the solution rather than being adsorbed onto the hydrate surfaces.

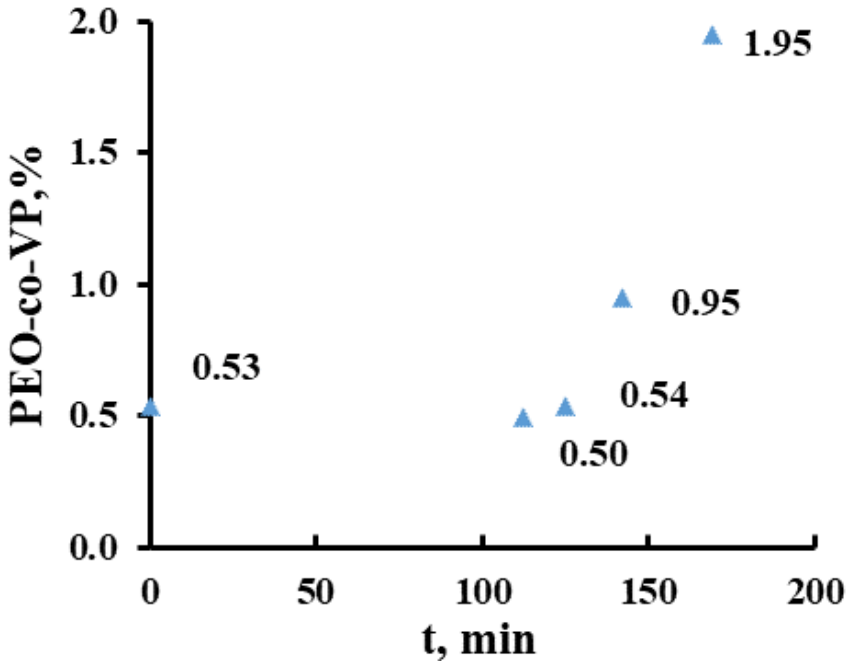

Fig. 4.7 PEO-co-VP concentration during hydrate growth in 0.5% PEO-co-VP + 15% MeOH solution

This is similar to the results of the hydrate-forming solution containing MEG, as seen in Figure 4.8. According to Shin *et al* (2013), the inhibition effect of polar molecules was not due to their destabilising effect on the solid clathrate hydrate framework but rather because of their ability to stabilise the guest molecules in the aqueous solution. This may be true also for the observations in this work. The results from this research have clearly demonstrated that the interaction of KHI with TIs (MEG or MeOH) is stronger than that of the KHI with the caged water molecules, or hydrates, leading to the increased KHI concentration in the liquid phases. When there is no TI present, a decrease in KHI concentration is shown, which is possibly due to the adsorption of KHI molecules onto the surfaces of hydrates as a result of the bonds between the carbonyls and hydrogen (Perrin et al., 2013). Similar observations have been reported by Foo *et al* (2016) and Zeng *et al* (2006).

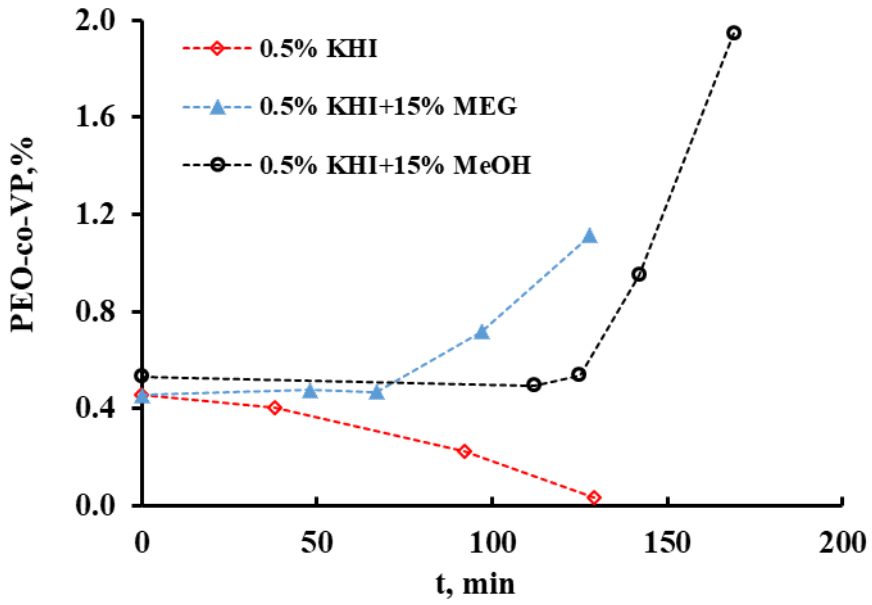

Fig. 4.8 KHI concentration during hydrate formation in 0.5% KHI, 0.5% KHI + 15% MEG and 0.5% KHI +15% MeOH solutions

4.2 The Effect of KHI Concentration on the Overall Performance of Synergists

To further investigate the contribution of PEO-co-VP towards the observed synergistic performance, the hydrate formation experiment was conducted with a fixed MeOH concentration of 10% and PEO-co-VP in concentrations of 0, 0.5%, 0.75% and 1%. The onset times, the growth times and the total gas consumption percentages for the above dosages are shown in Figures 4.9(a), (b) and (c). The subcooling temperature of solutions in the presence of 10% MeOH was over 8 °C regardless of the concentration difference of PEO-co-VP.

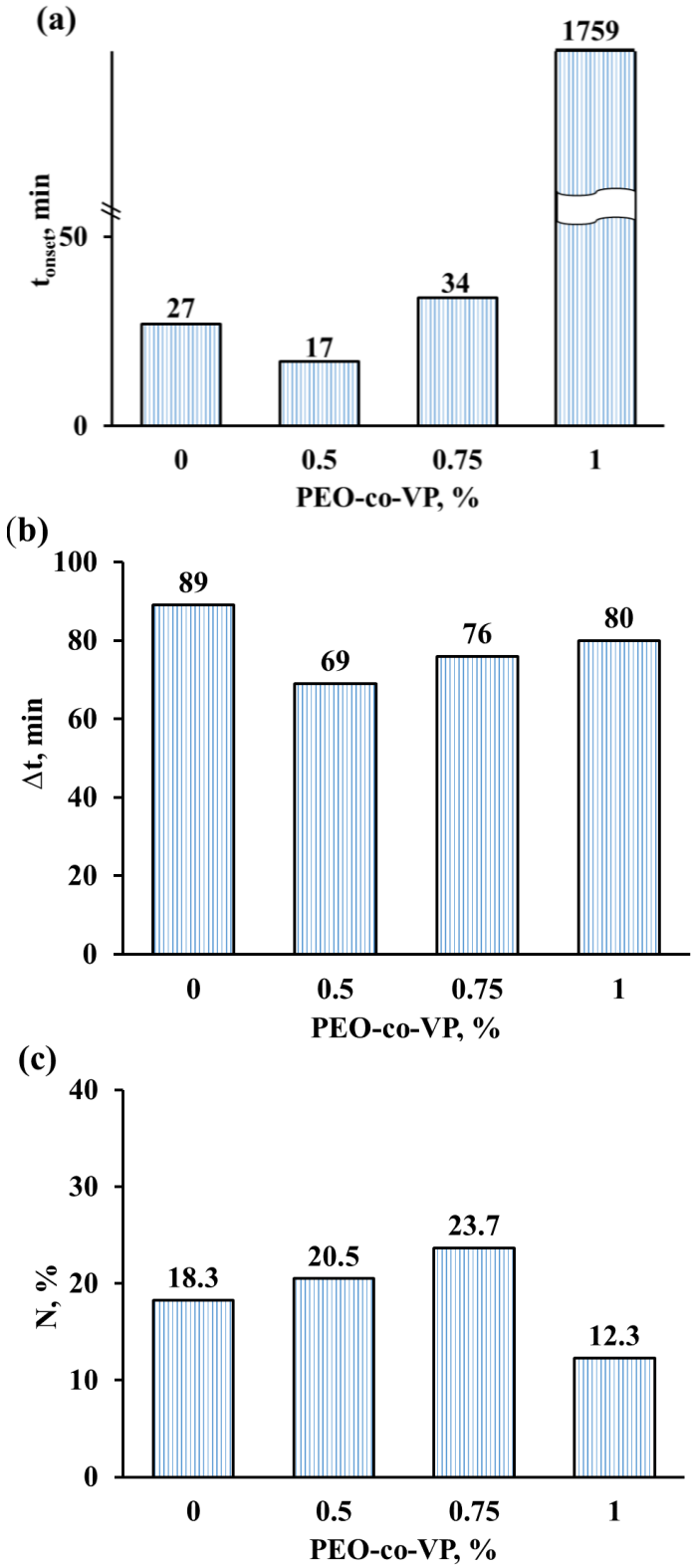

Fig. 4.9 The effects of PEO-co-VP on the synergistic performance of (a) onset time (t_{onset}), (b) growth time (Δt) and (c) the percentage of gas consumption (N) in the presence of 10% MeOH

As shown in Figure 4.9(a), the onset time demonstrates a clear ascending trend along with the increase in KHI concentration. For example, the onset time increases from 17 to 1,759 min when the KHI's concentration increases from 0.5% to 1%. There was no clear trend in changes for the growth time along with the change in polymer concentration (Fig. 4.9(b)). The longest growth time was 89 min, when no KHI was used. This was followed by growth times of 80, 76 and 69 min at the polymer concentrations of 1%, 0.75% and 0.5%, respectively. Similarly, the gas consumption data displayed in Figure 4.9(c) shows no clear pattern, although the added KHI did increase gas consumption.

As shown in Figure 4.10, the percentage of hydrate conversion was plotted against time to further investigate the relationship between hydrate growth and the concentration effect of PEO-co-VP. Overall, the slope of all systems is similar to that of the system with varying MeOH concentrations. The similar slope values indicate that a change in KHI concentration has little effect on the growth rate within the investigated range of concentrations.

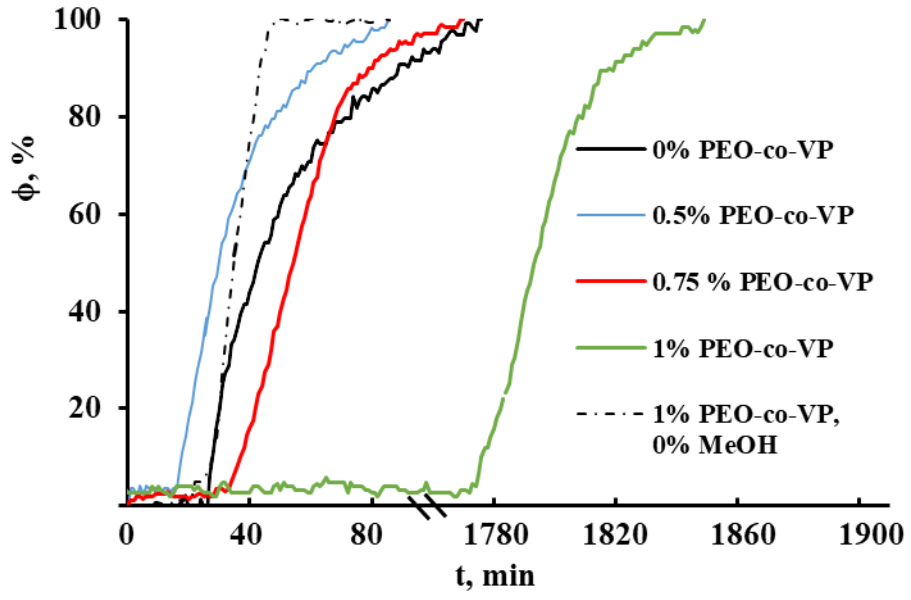

Fig. 4.10 Hydrate conversion (Ø) for 10% MeOH with varying PEO-co-VP concentrations

Hydrate formation within solutions containing 1% PEO-co-VP and 5% MeOH were tested at four pre-set temperatures, namely 2.0, 3.0, 4.0 and 5.2 °C. The operational conditions, including the pressure, the temperature, the corresponding subcooling temperature (T_{sc}), as well as the observed onset time (t_{onset}), growth time (Δt) and percentage of gas consumption (N) at the end of reactions are summarised in Table 4.2. The results of 2.0 °C are the average values from three repeated tests.

Table 4.2 Hydrate formation with 1% KHI + 5% MeOH at 2.0, 3.0, 4.0 and 5.2 °C

T_{set}, °C	P_{exp}, MPa	T_e, °C	T_{sc}, °C	t_{onset}, min	Δt, min	N, %
2.0	6.4	14.8(12.5)	12.8(10.5)	8±3	125±4	38.0±2.4
3.0	6.5	14.9(12.6)	11.9(9.6)	10	128	34.7
4.0	6.5	14.9(12.7)	10.9(8.7)	59	130	30.1
5.2	6.6	15.0(12.8)	9.8(7.6)	594	137	23.9

Data in parentheses represent the corresponding temperatures considering the TIs.

The results in Table 4.2 indicate that the onset time increases when the pre-set temperature (T_{set}) is raised. The onset times were 8, 10, 59 and 594 min at the set temperatures of 2.0, 3.0, 4.0 and 5.2 °C respectively. The increase in onset time was most significant when the temperature changed from 4.0 °C to 5.2 °C. The rise in pre-set temperature from 2.0 to 5.2 °C correlates with the reduction in subcooling from 12.8 to 9.8 °C (without consideration of the presence of MeOH), which reduced the driving force and increased the onset time (Anderson, et al., 2011). As shown in Figure 4.8, the relationship between t_{onset} and T_{sc} (K) fits the Arrhenius equation below, where R^2 is 0.95.

$$t_{onset} = \boldsymbol{a} \times e^{\frac{\boldsymbol{b}}{T_{sc}}}$$

As shown in Figure 4.11, the temperature effect on the onset time shows a similar trend for three hydrate-forming solutions, with consistent exponential correlations being

demonstrated between the onset time and subcooling temperature. It is apparent that, for the same onset time, the presence of 1% KHI sustained a significantly higher subcooling effect. The addition of 5% MeOH led to a further increase in subcooling but not to a large degree. When comparing the correlations between the t_{onset} and T_{sc}, as shown in Figure 4.11, it can be seen that the increase in onset time with the decrease in T_{sc} is more rapid for the formulation containing KHI or KHI + MeOH. For example, with the addition of 1% KHI, the onset time increased much more rapidly than for the blank within the same region of subcooling. This onset time was further extended with the addition of 5% MeOH.

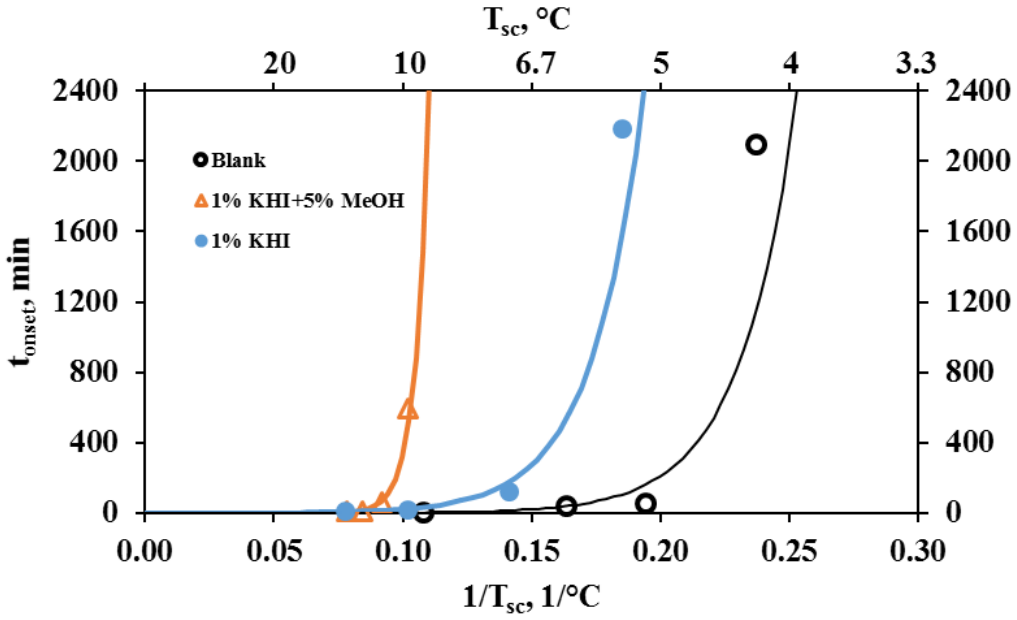

Fig. 4.11 Onset time versus subcooling temperature for 1% KHI + 5% MeOH, 1% KHI and the blank

The ***a*** and ***b*** values of all four dosages that were investigated in this study are summarised in Table 4.3. Both ***a*** and ***b*** values increased from the blank solution to the solutions with added KHI, KHI + MEG and KHI + MeOH, reflecting a more rapid increase in the onset time when mixed KHI and TI were used at the same subcooling temperature as the KHI alone.

Table 4.3 The value of ***a*** and ***b*** and the logarithm form of the fitted Arrhenius equation

KHI, %	TI, %	$\ln t_{onset} = \ln a + \frac{b}{T_{sc}}$	*a*	*b*
0	0	$-3.812 + \frac{45.80}{T_{sc}}$	0.022	45.80
1	0	$-1.865 + \frac{49.85}{T_{sc}}$	0.155	49.85
1	MEG, 5	$-2.293 + \frac{79.81}{T_{sc}}$	0.101	79.91
1	MeOH, 5	$-13.122 + \frac{190.85}{T_{sc}}$	$2x10^{-6}$	190.85

For the hydrate growth time (Table 4.2), the effect of the temperature was less noticeable. However, the percentage of gas consumption decreased with the increase in temperature (Fig. 4.12). This is in agreement with what has been observed for the hydrate-forming solution containing 1% KHI only, as shown in the same figure. It should be noted that there was little change in gas consumption for the system containing 1% KHI when the temperature was raised from 2.0 to 5.2℃ (35.3% at 2℃ and 37.1% at 5.2℃). However, in the presence of 5% MeOH, the consumption reduced from 38.0% to 23.9%, which further demonstrates the synergistic effect of the KHI and MeOH.

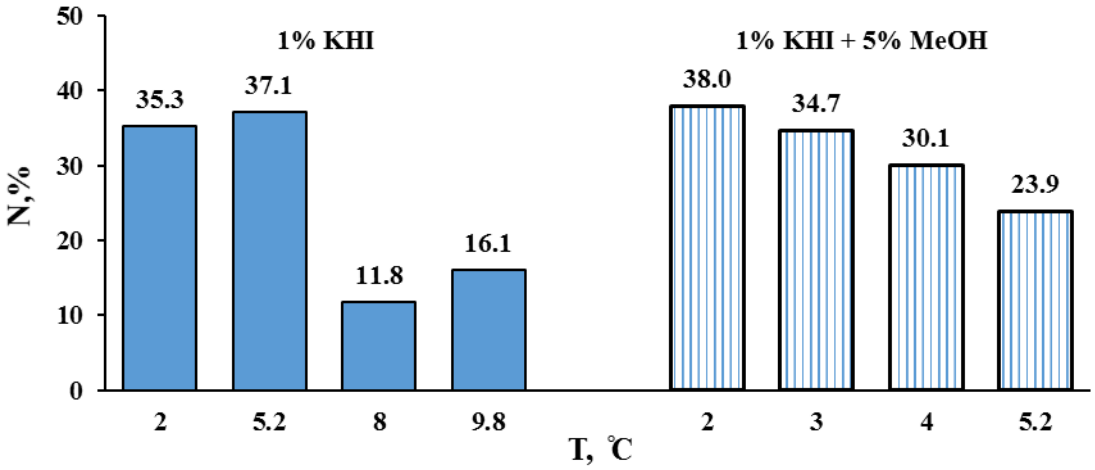

Fig. 4.12 Percentage of gas consumption (N) for 1% KHI and 1% KHI + 5% MeOH at various tested temperatures

When compared with the similar system containing the same mass percentage of MEG (see Table 3.2), MeOH showed a better synergistic effect with KHI at lower pre-set hydrate-forming temperatures (Fig. 4.13). In the presence of 5% MeOH, a longer onset time was achieved when compared with the systems containing 5% MEG at the same pre-set temperature. This is possibly due to the smaller size of the MeOH molecules making them more active than MEG when interacting with water molecules (Zhang et al., 2013).

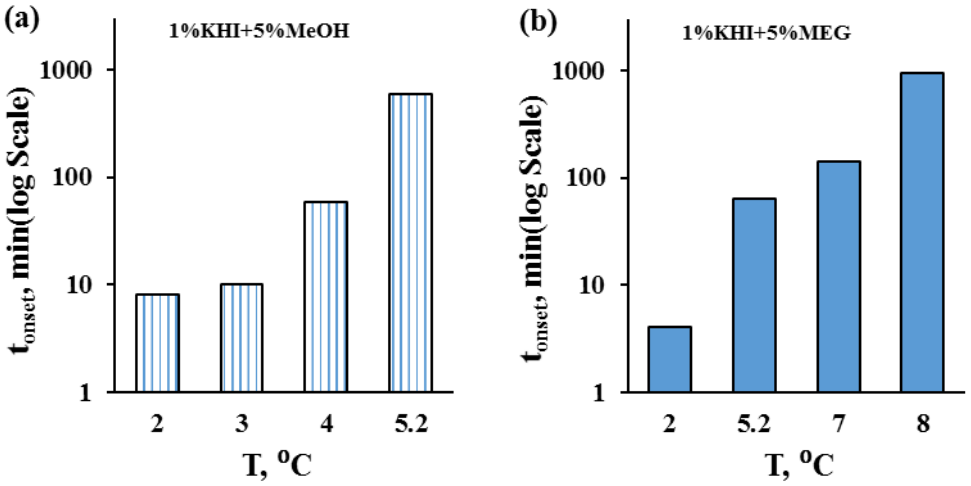

Fig. 4.13 Onset times for (a) 1% KHI + 5% MeOH and (b) 1% KHI + 5% MEG at various tested temperatures

4.3 Conclusions

This chapter focused on the investigation of the inhibition performance of KHI in the presence of MeOH. The synergistic effect was clearly demonstrated in the aspect of prolonged onset time and reduced gas consumption. The addition of 10% MeOH to PEO-co-VP (1%) significantly improved the hydrate inhibition performance compared with either 1% KHI alone or 10% MeOH in the absence of KHI.

Similar to the findings in Chapter 3, an increased concentration of KHI in the remaining liquid phase was observed. Therefore, it is speculated that the synergistic effect is due to the presence of MeOH, which assists the KHI molecules to remain in the liquid phase. The effect of subcooling in regard to the synergistic effect is similar to that of MEG on the KHI.

Chapter 5 Conclusions and Future Work

This work was conducted to investigate the synergistic effect of a KHI (PEO-co-VP) and two TIs (MEG and MeOH) on gas hydrate inhibition. MEG and MeOH were selected to work together with the KHI due to the consideration of their popularity and their easy accessibility in the field. The following conclusions were made according to the experimental observations.

Firstly, PEO-co-VP exhibited inhibition of the onset of hydrate formation at high subcooling temperatures. However, increased KHI concentrations resulted in reduced induction time due to the possible catastrophic hydrate growth at the investigated concentration range of 0.5-1.5%.

The onset time, in the presence of MEG and KHI, showed significant improvement when compared with the results of either MEG or KHI alone, demonstrating a strong synergistic effect. An increase in the synergistic effect was demonstrated by the increase of MEG concentration up to 15%. This is particularly true for those solutions containing 1% and 0.5% KHI. A slowing down of growth and a reduction in gas consumption were also observed. However, the result was not significant when compared with the increase in onset time.

The addition of MeOH showed a similar effect on the performance of PEO-co-VP. The synergistic effect was most clearly shown in the hydrate-forming solution that contained 1% KHI and 10% MeOH.

KHI concentrations in the liquid phase were tested during the stage of hydrate growth and were used to explain the mechanism of the synergistic effect. The concentration of KHI increased in the presence of the hydrate-forming solutions that contained either MeOH or MEG. This is different to the result for the system containing KHI only, which showed a downward trend. The improvement in the growth inhibition may possibly be attributable to the increased activities between inhibitors and water molecules due to their increased concentrations in the liquid phase.

Finally, a study of hydrate formation at different subcooling temperatures with different hydrate-forming solutions (the blank, KHI, KHI + TI) was used to quantify the synergistic effect. The subcooling temperature played a vital role in the inhibition of hydrate formation when any combination of KHI and TI was used.

This work has demonstrated the feasibility of applying a combination of thermodynamic and KHI inhibitors for gas hydrate inhibition at the laboratory scale. Further work using a flow loop will be a continuing project within our research group. Data reported from this project, including the KHI concentration change during the hydrate formation process, and the correlation established between the onset time and the subcooling temperature, are the first steps and they will have extended applications in this research field.

References

Anderson, R., Mozaffar, H., & B. Tohidi. 2011. Development of a crystal growth inhibition based method for the evaluation of kinetic hydrate inhibitors. Proceeding of the 7th International Conferennce on Gas Hydrate, Edinburgh, Scotland, U.K. Jun 17-21.

Akhfash, M., J. A. Boxall, Z. M. Aman, M. L. Johns, & E. F. May. 2013. Hydrate formation and particle distributions in gas–water systems. Chemical Engineering Science, 104, 177-188.

Arjmandi, M., S. Ren, J. Yang, & B. Tohidi. 2002. Design and testing of low dosage hydrate inhibitors. Paper presented at 4th International Conference on Gas Hydrates, 516-519.

Arjmandi, M., B. Tohidi, A. Danesh, & A. C. Todd. 2005. Is subcooling the right driving force for testing low-dosage hydrate inhibitors? Chemical engineering science, 60, 1313-1321.

Bera, A., K. Ojha, T. Kumar, & A. Mandal. 2012. Mechanistic study of wettability alteration of quartz surface induced by nonionic surfactants and interaction between crude oil and quartz in the presence of sodium chloride salt. Energy & Fuels, 26 (6), 3634-3643.

Brustad, S., K.-P. Løken, & J. G. Waalmann. 2005. Hydrate prevention using MEG instead of MeOH: impact of experience from major Norwegian developments on technology selection for injection and recovery of MEG. Proceedings of the Offshore Technology Conference, Huston, Texas, USA May 2–5.

Cha, M., K. Shin, J. Kim, D. Chang, Y. Seo, H. Lee, & S.-P. Kang. 2013. Thermodynamic and kinetic hydrate inhibition performance of aqueous ethylene glycol solutions for natural gas. Chemical Engineering Science, 99, 184-190.

Cha, M., K. Shin, Y. Seo, J.-Y. Shin, & S.-P. Kang. 2013. Catastrophic growth of gas hydrates in the presence of kinetic hydrate inhibitors. The Journal of Physical Chemistry A, 117 (51), 13988-13995.

Christiansen, R. L. & E. D. Sloan. 1994. Mechanisms and kinetics of hydrate formation. Annals of the New York Academy of Sciences, 715, 283-305.

Cohen, J. M., P. F. Wolf, & D. Young. 1998. Enhanced hydrate inhibitors: powerful synergism with glycol ethers. Energy & Fuels, 12, 216-218.

Daraboina, N., P. Linga, J. Ripmeester, V. K. Walker, & P. Englezos. 2011. Natural gas hydrate formation and decomposition in the presence of kinetic inhibitors. 2. stirred reactor experiments. Energy & Fuels, 25, 4384-4391

Daraboina, N., C. Malmos, & N. Von Solms. 2013. Synergistic kinetic inhibition of natural gas hydrate formation. Fuel, 108, 749-757.

Daraboina, N., C. Malmos, & N. Von Solms. 2013. Investigation of kinetic hydrate inhibition using a high pressure micro differential scanning calorimeter. Energy &.Fuels, 27 (10), 5779-5786.

Daraboina, N., S. Pachitsas, & N. Von Solms. 2015. Experimental validation of kinetic inhibitor strength on natural gas hydrate nucleation. Fuel, 139, 554-560.

Del Villano L., R. Kommedal, M. W. Fijten, U. S. Schubert, R. Hoogenboom, & M. A. Kelland. 2009. A Study of the kinetic hydrate inhibitor performance and seawater biodegradability of a series of poly(2-alkyl-2-oxazoline)s. Energy & Fuels, 23, 3665-3673.

Del Villano, L. & M. A. Kelland. 2010. An investigation into the kinetic hydrate inhibitor properties of two imidazolium-based ionic liquids on structure II gas hydrate. Chemical Engineering Science, 65, 5366-5372.

Del Villano, L. & M. A. Kelland. 2011. An investigation into the laboratory method for the evaluation of the performance of kinetic hydrate inhibitors using superheated gas hydrates. Chemical Engineering Science, 66, 1973-1985.

Ding, A., S. Wang, T. Pelemis, C. Crisafio, & X. Lou. 2010. Specific critical concentrations of low dosage hydrate inhibitors in a THF–NaCl hydrate formation solution. Asia-Pacific Journal of Chemical Engineering, 5, 577-584.

Englezos, P., N. Kalogerakis, P. D. Dholabhai, & P. R. Bishnoi. 1987. Kinetics of gas hydrate formation from mixtures of methane and ethane. Chemical Engineering Science, 42 (11), 2659-2666.

Englezos, P. 1993. Clathrate hydrates. Industrial & Engineering Chemistry Research, 32 (7), 1251-1274.

Foo, C. W., L. Ruan, & X. Lou. 2016. The inhibition performance in relation to the adsorption of a polymeric kinetic inhibitor towards THF hydrates in the presence of methanol, ethanol and monoethylene glycol. Journal of Natural Gas Science and Engineering, 35, 1587-1593

Giavarini, C. & K. Hester. 2011. Hydrates seen as a problem for the oil and gas industry. Gas Hydrate: Immerse energy potential and environtmental challengs, 97-116.

Huo, H. J., R. H. Wang, H. J. Ni, & Y. L. Liu. 2014. An experimental study on the synergetic effects of kinetic and thermodynamic gas hydrate inhibitors. Petroleum Science and Technology, 32, 1940-1947.

Jacobson, L. C., W. Hujo, & V. Molinero. 2010. Amorphous precursors in the nucleation of clathrate hydrates. Journal of the American Chemical Society, 132, 1806-11811.

Kashchiev, D. & A. Firoozabadi. 2003. Induction time in crystallization of gas hydrates. Journal of Crystal Growth, 250, 499-515.

Ke, W., T. M. Svartaas, & H. K. Abay. 2013. Effects of low concentration methanol, PVP and PVCap on structure-I methane hydrate formation. Journal of Energy and Power Engineering, 7, 432-439.

Ke, W., T. M. Svartaas, J. T. Kvaløy, & B. R. Kosberg. 2016. Inhibition–promotion: dual effects of polyvinylpyrrolidone (PVP) on structure-II hydrate nucleation. Energy & Fuels, 30 (9), 7646-7655.

Kelland, M. A., T. M. Svartaas, & L. A. Dybvik. 1995. A New Generation of Gas Hydrate Inhibitors. SPE Annual Technical Conference Proceedings, Dallas, TX, Paper No. SPE30695-MS.

Kelland, M. A. 2006. History of the development of low dosage hydrate inhibitors. Energy & Fuel, 20, 825-847.

Kelland, M. A., A. H. Kvæstad, & E. L. Astad. 2012. Tetrahydrofuran hydrate crystal growth inhibition by trialkylamine oxides and synergism with the gas kinetic hydrate inhibitor poly(N-vinyl caprolactam). Energy & Fuels, 26 (7), 4454-4464.

Kelland, M. A. 2014. Gas hydrate control. In Production Chemicals for the Oil and Gas Industry(2nd Ed., 219-258), CRC Press.

Kelland, M. A., A. Grinroed, & E. G. Dirdal. 2015. Novel benchtop wheel loop for low dosage gas hydrate inhibitor screening: comparison to rocking cells for a series of antiagglomerants. J. Chem. Eng. Data, 60(2), 252-257.

Kidnay, A. J. & W. R. Parrish. 2006. Field operations and inlet receiving. In Fundamentals of Natural Gas Processing (33-61), CRC Press, Florida.

Kim, J., K. Shin, Y. Seo, S. J. Cho, & J. D. Lee. 2014. Synergistic hydrate inhibition of monoethylene Glycol with poly(vinylcaprolactam) in thermodynamically underinhibited system. The Journal of Physical Chemistry B, 118, 9065-9075.

Kim, J., H. Kim, Y. Sohn, D. Chang, Y. Seo, & S. P. Kang. 2017. Prevention of methane hydrate re-formation in transport pipeline using thermodynamic and kinetic hydrate inhibitors. Journal of Petroleum Science and Engineering, 154, 114-125.

Kim, M., Y. W. Bae, B. Lee, I. W. Cheong, & K. Shin. 2018. LCST-Modulated polymers for synergistic hydrate inhibition in methane gas flowlines. Energy & Fuels, 32(3), 3013-3021.

King, H. E., J. L. Hutter, M. Y. Lin, & T. Sun. 2000. Polymer conformations of gas-hydrate kinetic inhibitors: A small-angle neutron scattering study. The Journal of Chemical Physics, 112 (5), 2523-2532.

Koh, C. A. 2002. Towards a fundamental understanding of natural gas hydrates. Chem. Soc. Rev., 31, 157-167.

Koh, C. A. & P. Creek. 2011. Safety in hydrate plug removal. In Natural Gas Hydrates in Flow Assurance (pp.37-48), Boston, Gulf Professional Publishing.

Kumar, R., J. D. Lee, M. Song, & P. Englezos. 2008. Kinetic inhibitor effects on methane/propane clathrate hydrate-crystal growth at the gas/water and water/n-heptane interfaces. Journal of Crystal Growth, 310 (6), 1154-1166.

Kuznetsova, T., A. Sapronova, B. Kvamme, K. Johannsen, & J. Haug. 2010. Impact of low-dosage inhibitors on clathrate hydrate Stability. Macromolecular Symposia, 287, 168-176.

Lederhos, J. P., J. P. Long, A. Sum, R. L. Christiansen, & E. D. Sloan Jr. 1996. Effective kinetic inhibitors for natural gas hydrates. Chemical Engineering Science, 51, 1221-1229.

Leporcher, E. M., J. M. Fourest, C. Labes-Carrier, & M. Lompre. 1998. Multiphase transportation: A Kinetic inhibitor replaces methanol to prevent hydrates in a 12-inc. pipeline. Proceeding of the European Petroleum Conference, La Hague, France

Lafond, P. G., K. A. Olcott, E. D. Sloan, C. A. Koh, & A. K. Sum. 2012. Measuremetn of methane hydrate equilibrium in systems inhibited with NaCl and methanol. J. Chem. Termodyn.,48, 1-6.

Li, X., L. Negadi, & A. Firoozabadi. 2010. Anti-agglomeration in cyclopentane hydrates from bio- and co-surfactants. Energy & Fuel, 24, 4937-4943.

Lopez-Echeverry, J. S., S. Reif-Acherman, & E. Araujo-Lopez. 2017. Peng-Robinson equation of state: 40 years through cubics. Fluid Phase Equilibria, 447, 39-71.

Lou, X., A. Ding, N. Maeda, S. Wang, K. Kozielski, & P. G. Hartley. 2012. Synthesis of effective kinetic inhibitors for natural gas hydrate. Energy & Fuels, 26, 1037-1043.

Luna-Ortiz, E., M. Healey, R. Anderson, & E. Sørhaug. 2014. Crystal growth inhibition studies for the qualification of a kinetic hydrate inhibitor under flowing and shut-In conditions. Energy & Fuels, 28, 2902-2913.

Maeda, N. 2015. Is the surface of gas hydrates dry? Energies, 8 (6), 5361-5369.

Magnusson, C. D., & M. A. Kelland. M. A. 2014. Study on the Synergistic Properties of Quaternary Phosphonium Bromide Salts with N-Vinylcaprolactam Based Kinetic Hydrate Inhibitor Polymers. Energy & Fuels, 28(11), 6803-6810.

Makogon, Y., T. Makogon, & S. Holditch. 2000. Kinetics and mechanisms of gas hydrate formation and dissociation with inhibitors. Annals of the New York Academy of Sciences, 912, 777-796.

Mokhatab, S., R. J. Wilkens, & K. J. Leontaritis. 2007. A review of strategies for solving gas-hydrate problems in subsea pipelines. Energy Sources, Part A, 29, 39-45.

Moradpour, H., A. Chapoy, & B. Tohidi. 2011. Transportability of hydrate particles at high water cut systems and optimisation of anti-agglomerant concentration. Proceedings of the 7th International Conference on Gas Hydrates, Edinburgh, Scotland, United Kingdom, Jul. 17-21.

Mozaffar, H., R. Anderson, & B. Tohidi. 2016. Effect of alcohols and diols on PVCap-induced hydrate crystal growth patterns in methane systems. 2016. Fluid Phase Equilibria, 425, 1-8.

Nakarit, C., M. A. Kelland, D. Liu, & E. Y.-X. Chen. 2013. Cationic kinetic hydrate inhibitors and the effect on performance of incorporating cationic monomers into N-vinyl lactam copolymers. Chemical Engineering Science, 102, 424-431.

Nakayama, H., D. H. Brouwer, Y. P. Handa, D. D. Klug, J. S. Tse, C. I. Ratcliffe, X. Zhu, & J. A. Ripmeester. 1997. Methanol: clathrate hydrate former or inhibitor? ACS Division of Fuel Chemistry, 42 (1), 516-520.

Olsen, R., B. Kvamme, & T. Kuznetsova. 2017. Hydrogen bond lifetimes and statistics of aqueous mono-, di- and tri-ethylene glycol. AIChE Journal, 63 (5), 1674-1689.

Park, J., H. Lee, Y. Seo, W. Tian, & C. D. Wood. 2016. Performance of polymer hydrogels incorporating thermodynamic and kinetic hydrate inhibitors. Energy & Fuels, 30 (4), 2741-2750.

Perrin, A., O. M. Musa, & J. W. Steed. 2013. The chemistry of low dosage clathrate hydrate inhibitors. Chemical Society Reviews, 42, 1996-2015.

Patel, Z. D. & J. Russum. 2010, Jun. 24. Chemical inhibition of gas hydrates in deepwater production systems. Offshore. Retrieved from http:// www.offshore-mag.com

Peytavy, J.-L., P. Glénat, & P. Bourg. 2008. Qualification of low dose hydrate inhibitors (LDHIs): field cases studies demonstrate the good reproducibility of the results obtained from flow loops. Proceedings of the 6th International Conference on Gas Hydrates, Vancouver, British Columbia, Canada, Jul. 6-10.

Qin, H. B., C. Y. Sun, Z. F. Sun, B. Liu, & G. J. Chen. 2016. Relationship between the interfacial tension and inhibition performance of hydrate inhibitors. Chem. Eng. Sci., 148, 182−189.

Radhakrishnan, R. & B. L. Trout. 2012. A new approach for studying nucleation phenomena using molecular simulations: application to CO_2 hydrate clathrates. The Journal of Chemical Physics, 2002(117), 1786-1796.

Sa, J.-H., G.-H. Kwak, K. Han, D. Ahn, S. J. Cho, J. D. Lee, & K.-H. Lee. 2016. Inhibition of methane and natural gas hydrate formation by altering the structure of water with amino acids. Scientific reports, 6.

Semenov, A. P., V. I. Medvedev, P. A. Gushchin, & V. S. Yakushev. 2015. Effect of heating rate on the accuracy of measuring equilibrium conditions for methane and argon hydrates. Chemical Engineering Science, 137, 161-169.

Sharifi, H., J. Ripmeester, V. K. Walker, & P. Englezos. 2014. Kinetic inhibition of natural gas hydrates in saline solutions and heptane. Fuel, 117, Part A, 109-117.

Sharifi, H. & P. Englezos. 2015. Accelerated hydrate crystal growth in the presence of low dosage additives known as kinetic hydrate inhibitors. Journal of Chemical & Engineering Data, 60, 336-342.

Shin, K., K. A. Udachin, I. L. Moudrakovski, D. M. Leek, S. Alavi, C. I. Ratcliffe, & J. A. Ripmeester. 2013. Methanol incorporation in clathrate hydrates and the implications for oil and gas pipeline flow assurance and icy planetary bodies. Proceedings of the National Academy of Sciences, 110 (21), 8437-8442.

Sloan, E. D., & F. A. Fleyfel. 1991. A molecular mechanism for gas hydrate nucleation from ice. AIChE J., 37 (9), 1281−1292.

Staykova, D. K., W. F. Kuhs, A. N. Salamatin, & T. Hansen. (2003). Formation of porous gas hydrates from ice powders: diffraction experiments and multistage model. The Journal of Physical Chemistry B, 107(37), 10299-10311.

Sun, M., Y. Wang, & A. Firoozabadi. 2012. Effectiveness of alcohol cosurfactants in hydrate antiagglomeration. Energy & Fuels, 26, 5626-5632.

Szymczak, S., K. B. Sanders, M. K. Pakulski, & T. D. Higgins. 2005. Chemical compromise: a thermodynamic and low-dose hydrate-inhibitor solution for hydrate control in the Gulf of Mexico. SPE-96418-MS, presented at SPE Annual Technical Conference and Exhibition, Dallas, Texas.

Talaghat, M. R. 2013. Prediction of induction time for natural gas components during gas hydrate formation in the presence of kinetic hydrate inhibitors in a flow mini-loop apparatus. The Canadian Journal of Chemical Engineering, 91, 790-797.

Talaghat, M. R. 2014. Enhancement of the performance of modified starch as a kinetic hydrate inhibitor in the presence of polyoxides for simple gas hydrate formation in a flow mini-loop apparatus. Journal of Natural Gas Science and Engineering, 18, 7-12.

Tariq, M., D. Rooney, E. Othman, S. Aparicio, M. Atilhan & M. Khraisheh. 2014. Gas hydrate inhibition: a review of the role of ionic liquids. Industrial & Engineering Chemistry Research, 53, 17855-17868.

Tohidi, B., R. Anderson, R, A. Chapoy, J. Yang, & R. W. Burgass. 2012. Do we have new solutions to the old problem of gas hydrates? Energy & Fuels, 26 (7), 4053-4058.

Tohidi, B., R. Anderson, H. Mozaffar, & F. Tohidi. 2014. The return of kinetic hydrate inhibitors. Energy & Fuels, 29 (12), 8254-8260.

Veluswamy, H. P., A. Kumar, Y. Seo, J. D. Lee, & P. Linga. 2018. A review of solidified natural gas (SNG) technology for gas storage via clathrate hydrates. Applied Energy, 216, 262-285.

Verrett, J., D. Posteraro, & P. Servio. 2012. Surfactant effects on methane solubility and mole fraction during hydrate growth. Chemical Engineering Science, 84, 80-84.

Wakisaka, A., H. Abdoul-Carime, Y. Yamamoto, & Y. Kiyozumi. 1998. Non-ideality of binary mixtures water-methanol and water-acetonitrile from the viewpoint of clustering structure. Journal of the Chemical Society, Faraday Transactions, 94 (3), 369-374.

Yagasaki, T., M. Matsumoto, & H. Tanaka. 2015. Adsorption mechanism of inhibitor and guest molecules on the surface of gas hydrates. Journal of the American Chemical Society, 137, 12079-12085.

York, J. D., & A. Firoozabadi. 2008. Alcohol cosurfactants in hydrate antiagglomeration. The Journal of Physical Chemistry B, 112, 10455-10465.

Zare, M., A. Haghtalab, A. N. Ahmadi, K. Nazari, & A. Mehdizadeh. 2015. Effect of imidazolium based ionic liquids and ethylene glycol monoethyl ether solutions on the kinetic of methane hydrate formation. Journal of Molecular Liquids, 204, 236-242.

Zeng, H., L. Wilson, V. Walker, & J. Ripmeester. 2006. Effect of antifreeze proteins on the formation and reformation of tetrahydrofuran clathrate hydrate. Journal of the American Chemical Society, 128, 2844-2850.

Zhang, N., W. Li, C. Chen, J. Zuo, & L. Weng. 2013. Molecular dynamics study on water self-diffusion in aqueous mixtures of methanol, ethylene glycol and glycerol: investigations from the point of view of hydrogen bonding. Molecular Physics, 111 (7), 939-949.

Zhao, X., Z. Qiu, G. Zhou, & W. Huang. 2015. Synergism of thermodynamic hydrate inhibitors on the performance of poly (vinyl pyrrolidone) in deepwater drilling fluid. Journal of Natural Gas Science and Engineering, 23, 47-54.

Appendix A:

Onset time (t_{onset}) and the corresponding subcooling temperature (T_{sc}) of various hydrate-forming solutions

	Blank						1% KHI						1% KHI + 5% MEG						1% KHI + 5% MeOH					
T_{set}	P, MPa	Gas, mole	Water, mole	T_{eq}, °C,	T_{sc}, °C	t_{onset}, min	P, MPa	Gas, mole	Water, mole	T_{eq}, °C,	T_{sc}, °C	t_{onset}, min	P, MPa	Gas, mole	Water, mole	T_{eq}, °C,	T_{sc}, °C	t_{onset}, min	P, MPa	Gas, mole	Water, mole	T_{eq}, °C,	T_{sc}, °C	t_{onset}, min
							6.41	0.57		14.9	12.86	17							6.46	0.57		14.87	12.87	11
2.0							6.44	0.57	1.59	14.9	12.89	10	6.39	0.56	1.59	14.85	12.84	4	6.40	0.55	1.70	14.79	12.79	8
							6.42	0.57		14.9	12.86	8							6.34	0.55		14.73	12.73	6
3.0																			6.46	0.56	1.70	14.87	11.87	10
4.0																			6.50	0.56	1.70	14.91	10.91	59
							6.54	0.57		15.0	9.81	16												
5.2							6.55	0.57	1.59	15.0	9.81	18	6.51	0.56	1.59	14.96	9.76	63	6.60	0.56	1.70	15.02	9.82	594
							6.52	0.57		15.0	9.78	17												
5.7	6.52	0.57	1.61	15.0	9.3	4																		
7.0													6.60	0.56	1.59	15.07	8.07	140						
8.0							6.62	0.57	1.59	15.1	7.08	119	6.54	0.56	1.59	15.10	7.10	942						
9.0	6.65	0.57	1.61	15.1	6.1	43																		
9.8							6.73	0.57	1.59	15.2	5.40	2187												
10.0	6.67	0.57	1.61	15.2	5.2	60																		
11.0	6.74	0.57	1.61	15.2	4.2	2102																		

Appendix B:

Onset time (t_{onset}) and the corresponding subcooling temperature (T_{sc}) of various hydrate-forming solutions at 2 °C

KHI, %	TI, %	P, MPa	T_e, °C	T_{sc}, °C	Gas, mole	Water, mole	t_{onset}, min	Δt, min	N, %
0	0	6.39	14.86	12.86	0.56	1.61	0	108	49.6
		6.38	14.85	12.85	0.56		0	145	48.9
		6.36	14.82	12.82	0.56		0	127	44.4
0	MEG, 15	6.44	14.65(10.87)	12.65(8.87)	0.57	1.36	57	98	18.5
0.5	0	6.27	14.71	12.71	0.55	1.60	16	64	37.6
		6.35	14.80	12.80	0.56		21	70	36.1
		6.42	14.88	12.88	0.57		26	94	34.4
0.5	MEG, 1.5	6.47	14.91(14.59)	12.91(12.59)	0.57	1.57	20	71	35.0
		6.41	14.83(14.51)	12.83(12.51)	0.56		15	70	34.7
		6.39	14.82(14.51)	12.82(12.51)	0.56		14	67	34.7
0.5	MEG, 3	6.46	14.88(14.24)	12.88(12.24)	0.57	1.55	56	38	20.2
		6.46	14.87(14.22)	12.87(12.22)	0.57		17	73	29.1
		6.36	14.76(14.11)	12.76(12.11)	0.57		21	84	29.5
0.5	MEG, 10	6.47	14.75(12.40)	12.75(10.40)	0.54	1.67	57	47	24.0
		6.36	14.61(12.28)	12.61(10.28)	0.53		51	94	29.0
		6.42	14.71(12.36)	12.71(10.36)	0.54		42	80	24.1
0.5	MEG, 15	6.31	14.46(10.65)	12.46(8.65)	0.53	1.62	95	127	14.1
0.75	MEG, 15	6.43	14.57(10.74)	12.57(8.74)	0.54	1.61	130	166	10.3

KHI, %	TI, %	P, MPa	T_e, °C	T_{sc}, °C	Gas, mole	Water, mole	t_{onset}, min	Δt, min	N, %
1	No TI	6.41	14.86	12.86	0.57	1.59	17	68	32.2
		6.44	14.90	12.90	0.57		10	70	36.4
		6.42	14.86	12.86	0.57		8	79	37.4
1	MEG, 1.5	6.40	14.84(14.53)	12.84(12.53)	0.56	1.58	6	68	35.2
1	MEG,5(4.7)	6.41	14.75(13.70)	12.75(11.70)	0.56	1.56	16	182	23.8
		6.38	14.34(13.30)	12.34(11.30)	0.55	1.76	18	170	31.7
		6.36	14.33(13.28)	12.33(11.28)	0.54	1.76	19	119	25.6
1	MEG,10	6.37	14.64(12.26)	12.64(10.26)	0.54	1.66	322	174	29.7
1	MEG, 15	6.30	14.46(10.62)	12.46(8.62)	0.54	1.56	-	-	-
1.5	No TI	6.41	14.84	12.84	0.57	1.58	7	127	43.3
		6.42	14.85	12.85	0.57		5	90	48.7
		6.38	14.82	12.82	0.56		1	115	59.9
0	MeOH, 10	6.50	14.79(10.12)	12.79(8.12)	0.56	1.58	27	89	18.3
0	MeOH, 15	6.37	14.57(7.27)	12.57(5.27)	0.56	1.36	36	96	14.1
0.5	MeOH, 0.75	6.37	14.81(14.49)	12.81(12.49)	0.56	1.59	14	103	35.7
		6.39	14.83(14.51)	12.83(12.51)	0.56		6	47	34.1
		6.44	14.88(14.56)	12.88(12.56)	0.57		31	44	34.8
0.5	MeOH, 10	6.46	14.76(10.08)	12.76(8.08)	0.56	1.67	17	69	20.5
0.5	MeOH, 15	6.41	14.60(7.24)	12.60(5.24)	0.55	1.35	47	75	10.1
0.75	MeOH, 10	6.41	14.69(10.02)	12.69(8.02)	0.55	1.67	34	76	23.7

KHI, %	TI, %	P, MPa	T_e, °C	T_{sc}, °C	Gas, mole	Water, mole	t_{onset}, min	Δt, min	N, %
1	MeOH, 10	6.39	14.67(9.99)	12.68(7.99)	0.57	1.43	1759	80	12.3

The corresponding data considering TI is included in the parentheses.

Appendix C:

Copyright agreement for Chapter 1

ELSEVIER LICENSE
TERMS AND CONDITIONS

Nov 08, 2018

This Agreement between Curtin Univeristy -- XINYU LI ("You") and Elsevier ("Elsevier") consists of your license details and the terms and conditions provided by Elsevier and Copyright Clearance Center.

License Number	4464250796859
License date	Nov 08, 2018
Licensed Content Publisher	Elsevier
Licensed Content Publication	Chemical Engineering Science
Licensed Content Title	Effective kinetic inhibitors for natural gas hydrates
Licensed Content Author	J.P. Lederhos,J.P. Long,A. Sum,R.L. Christiansen,E.D. Sloan
Licensed Content Date	Apr 1, 1996
Licensed Content Volume	51
Licensed Content Issue	8
Licensed Content Pages	9
Start Page	1221
End Page	1229
Type of Use	reuse in a thesis/dissertation
Portion	figures/tables/illustrations
Number of figures/tables/illustrations	1
Format	both print and electronic
Are you the author of this Elsevier article?	No
Will you be translating?	No
Original figure numbers	Fig. 1
Title of your thesis/dissertation	The Inhibition Performance of Poly(ethyleneoxide-co-vinylpyrrolidone) in the Presence of Thermodynamic Hydrate Inhibitors
Expected completion date	Jun 2018
Estimated size (number of pages)	84
Requestor Location	Curtin Univeristy 15 Kirwan Way Winthrop, Western Australia 6150 Australia Attn: XINYU LI
Publisher Tax ID	GB 494 6272 12
Total	0.00 AUD
Terms and Conditions	

ELSEVIER LICENSE
TERMS AND CONDITIONS

Jun 20, 2018

This Agreement between Curtin Univeristy -- XINYU LI ("You") and Elsevier ("Elsevier") consists of your license details and the terms and conditions provided by Elsevier and Copyright Clearance Center.

License Number	4371811319295
License date	Jun 18, 2018
Licensed Content Publisher	Elsevier
Licensed Content Publication	The Journal of Chemical Thermodynamics
Licensed Content Title	Measurements of methane hydrate equilibrium in systems inhibited with NaCl and methanol
Licensed Content Author	Patrick G. Lafond,Kyle A. Olcott,E. Dendy Sloan,Carolyn A. Koh,Amadeu K. Sum
Licensed Content Date	May 1, 2012
Licensed Content Volume	48
Licensed Content Issue	n/a
Licensed Content Pages	6
Start Page	1
End Page	6
Type of Use	reuse in a thesis/dissertation
Portion	figures/tables/illustrations
Number of figures/tables/illustrations	1
Format	both print and electronic
Are you the author of this Elsevier article?	No
Will you be translating?	No
Original figure numbers	Fig 6
Title of your thesis/dissertation	The Inhibition Performance of Poly(ethyleneoxide-co-vinylpyrrolidone) in the Presence of Thermodynamic Hydrate Inhibitors
Expected completion date	Jun 2018
Estimated size (number of pages)	84
Requestor Location	Curtin Univeristy 15 Kirwan Way Winthrop, Western Australia 6150 Australia Attn: XINYU LI
Publisher Tax ID	GB 494 6272 12
Total	0.00 USD
Terms and Conditions	

Copyright agreement for Chapter 4

Thank you for your message. Permission is granted for your use of the material as described in your request. Please include a full citation for the original PNAS article when reusing the material. Because this material published after 2008, a copyright note is not needed. There is no charge for this material, either. Let us know if you have any questions.

Sincerely,

Kay McLaughlin for
Diane Sullenberger
PNAS Executive Editor

From: Lisa Li <xinyu.li1@postgrad.curtin.edu.au>
Sent: Wednesday, November 07, 2018 12:37 AM
To: PNAS Permissions <PNASPermissions@nas.edu>
Subject: re-use fig in my thesis

Hi:
I wrote to apply the permission of using fig from below article in my thesis work. Would you please advise what step I need to follow? Please see request information filled below.

Cheers
Lisa Li

1. Your full name, affiliation, and title

   XINYU LI, Curtin University, HDR student

2. Your complete mailing address, phone number, and email

   15 kirwan Way Winthrop WA6150 Australia

   xinyu.li1@postgrad.curtin.edu.au

   phone:61422760448

3. PNAS volume number, issue number, and issue date

   Vol.110 No. 21 , 21 May 2013

4. PNAS article title

   Methanol incorporation in clathrate hydrates and the implications for oil and gas pipeline flow assurance and icy planetary bodies.